5 VARIABLES AFFECTING MINIMUM DETECTABLE CONCENTRATIONS IN THE FIELD

Surface activity levels are assessed by converting detector response, through the use of a calibration factor, to radioactivity. Once the detector has been calibrated and an instrument efficiency (ϵ_i) established, several factors must still be carefully considered when using that instrument in the field. These factors involve the background count rate for the particular surface and the surface efficiency (ϵ_s), which addresses the physical composition of the surface and any surface coatings. Ideally, the surveyor should use experimentally determined surface efficiencies for the anticipated field conditions. The surveyor needs to know how and to what degree these different field conditions can affect the sensitivity of the instrument. A particular field condition may significantly affect the usefulness of a particular instrument (e.g., wet surfaces for alpha measurements or scabbled surfaces for low-energy beta measurements).

One of the more significant implicit assumptions commonly made during instrument calibration and subsequent use of the instrument in the field is that the composition and geometry of contamination in the field is the same as that of the calibration source. This may not be the case, considering that many calibration sources are fabricated from materials different from those that comprise the surfaces of interest in the field—e.g., activity plated on a metallic disc (Walker 1994). This difference usually manifests itself in the varying backscatter characteristics of the calibration and field surface materials.

Generally, it will not be necessary to recalculate the instrument MDC to adjust for the field conditions. For most of the items discussed below, the detection limit (in net counts or net count rate) remains the same, but the MDC may be different (due to the varying ϵ_s). In this study, the effects of typically encountered surface types and field conditions were evaluated quantitatively. These are discussed in the following sections.

5.1 Background Count Rates for Various Materials

Several different types of surface materials may be encountered in a facility undergoing decommissioning. Among the typical surface materials that were evaluated in this study were (a) brick, (b) ceramic block, (c) ceramic tile, (d) concrete block, (e) unpainted drywall, (f) vinyl floor tile, (g) linoleum, (h) steel, (i) wood pine treated with a commercially available water sealant product, and (j) untreated pine. The main difference considered was the background activity associated with each of these types of surface materials. In most cases, the background count rate for that type of surface needs to be determined and a new MDC established, provided that the specific surface type was not considered in the initial evaluation of the instrument's MDC.

Ambient background count rates were initially determined for gas proportional, ZnS scintillation, GM, and NaI scintillation detectors. Three variations were used for the gas proportional detectors: (a) detection of alpha radiation only (using a high voltage setting that discriminated all beta pulses), (b) detection of beta radiation only (using sufficient window density thickness to block alpha radiation), and (c) detection of alpha and beta radiation. Results of ambient background count rates are in Table 5.1. The ambient backgrounds were determined at the same location for all the tested surface materials and, as such, the ambient background was sometimes greater than a particular surface material background. This result was considered acceptable because a primary objective of this study was to evaluate detector responses in as close to field

conditions as possible.

Background count rates were obtained for ten surface materials using the same instrument/ detector combinations that were used to determine the ambient background. In general, background count rates were lowest for the linoleum, carbon steel, and wood, and highest for the brick and ceramic materials (Table 5.1). These background count rates will vary depending on the local area background radiation levels; however, the data provide information on the relative backgrounds in common construction materials.

MDCs for the gas proportional detectors operated in both the alpha-only and beta-only modes were calculated for each of the surface materials assuming a total efficiency (ϵ_{tot}) of 0.20 and 0.25 count per disintegration, for alpha and beta, respectively (Table 5.2). The MDCs were calculated from Equation 3-10, using the background count rates presented in Table 5.1. The MDCs in the alpha-only mode ranged from 28 to 83 dpm/100 cm^2, while the MDCs in the beta-only mode ranged from 268 to 425 dpm/100 cm^2. Since the detector MDC varies directly with the background count rate, the lowest MDCs were obtained for linoleum, carbon steel and wood, and concrete block and drywall, while the highest MDCs were for brick and ceramic materials. Figures 5.1 and 5.2 illustrate the effect of surface material background count rates on detector MDC for the gas proportional detectors operated in both the alpha-only and beta-only modes, respectively. These figures demonstrate the importance of carefully assessing the alpha background for various surface materials due to the wide range of MDC values. This is in contrast to the beta MDCs, which are fairly consistent for all materials examined, with the notable exception of brick and ceramics. In application, it is important that the surveyor establish specific material backgrounds that are representative of the surface types and field conditions.

The reader is referred to NUREG-1501, "Background as a Residual Radioactivity Criterion for Decommissioning," for additional information on background radionuclide concentrations.

5.2 Backscatter Effects

An experiment was performed to evaluate the backscatter characteristics of surfaces commonly encountered during the course of performing decommissioning surveys and to address their effect on surface activity assessments. A thin sheet of Mylar (0.22 mg/cm^2) was stretched across a metal frame with an area of approximately 126 cm^2. Two milliliters of a liquid SrY-90 radionuclide standard was deposited on the Mylar and allowed to air dry—about 4,100 dpm was deposited on the Mylar sheet. Measurements were then performed on various surfaces with the same activity-spiked Mylar sheet positioned between the surface of interest and the gas flow proportional detector. With this experimental setup, any differences in the detector response are solely attributable to the differences due to backscattered radiation. Gas flow proportional detectors were used to make surface activity measurements using both 0.4 and 3.8 mg/cm^2 window thicknesses. Table 5.3 depicts the different total efficiencies—determined by dividing the net count rate by deposited activity —obtained for the various surfaces used in this experiment. The efficiency data were normalized to the efficiency in air, which was assumed to produce negligible backscatter radiation. The backscatter factor, calculated by dividing the particular surface material efficiency by the efficiency in air, ranged from 1.20 to 1.43 for the detector with 0.4 mg/cm^2 window thickness, and ranged from 1.11 to 1.37 for the detector with 3.8 mg/cm^2 window thickness. Of particular interest is the backscatter factor for stainless steel—which is

often the substrate material for calibration sources—as compared to the other surfaces. For the detector with 0.4 mg/cm^2 window thickness, the backscatter factor for stainless steel was 1.43, as compared to 1.20 for wood, 1.24 for drywall, 1.25 for a tile floor, and 1.30 for sealed concrete floor. Thus, efficiencies for surfaces other than stainless steel may be overestimated by 10 to 20% due to the backscatter effect alone (the efficiency overestimation for the 3.8 mg/cm^2 window thickness ranged from 11 to 24%). The relatively high efficiency obtained with stainless steel calibration sources may result in the surface activity for surfaces like wood, drywall and concrete being underestimated by 10 to 20%. Furthermore, the total efficiency for SrY-90 on stainless steel versus concrete surfaces exhibit similar differences (about 10%) when the SrY-90 source was deposited on each of these surfaces (discussed in Section 5.5 and shown in Table 5.29).

5.3 Effects of Surface Condition on Detection Sensitivity

The conversion of the surface emission rate to the activity of the contamination source is often a complicated task that may result in significant uncertainty if there are deviations from the assumed source geometry. For example, consider the measurement error associated with an alpha surface activity measurement on a rough surface, such as scabbled concrete, where substantial attenuation reduces the count rate as compared to the calibration performed on the smooth surface of a National Institute of Standards and Technology (NIST) traceable source.

The effects of surface condition on detection sensitivity were evaluated for surfaces commonly encountered during decommissioning surveys. The surfaces studied were abraded (scabbled) concrete, finished (sealed) concrete, carbon steel, stainless steel, and wood. The results of this study provide a quantitative range of how various surface conditions may affect the detectability of various contaminants.

5.3.1 Surface Preparation

For this study, known quantities of NIST traceable Tc-99 and Th-230 standard sources, in aqueous solutions, were dispensed on each of the surfaces. The preparation of the reference sources from the traceable solution involved measurement uncertainties (e.g., pipetting errors, volumetric determinations) that were propagated into the overall statement of uncertainty.

Background count rates were obtained for instrument/surface combinations that were used to determine the surface activity measurements, so that the proper background could be subtracted from the gross counts. For the surface materials studied, the Tc-99 and Th-230 were dispensed to simulate both a point source and distributed source geometry (it should be noted that the Tc-99 and Th-230 were not mixed, but were dispensed on separate areas of each surface). The areal extent of the point source activity ranged from approximately 4 to 10 cm^2, while the distributed source geometry was fabricated by uniformly depositing droplets of the Tc-99 and Th-230 activity over a larger area (126 cm^2). The total Tc-99 activity dispensed in the point source geometry was 2828 ± 91 dpm (5660 ± 110 dpm for the sealed concrete), while 4595 ± 79 dpm of Th-230 was dispensed in a point source geometry. The Tc-99 and Th-230 activity dispensed in the distributed source geometry was 2830 ± 100 dpm and 4600 ± 170 dpm, respectively. Once dispensed, the radioactive material was allowed to dry overnight in a ventilated hood.

Uniformity measurements with a GM detector for distributed sources were performed to evaluate

how well the activity was spread over the surfaces (refer to Section 5.4.1 for a detailed description of uniformity measurements). It was important that the activity was precisely distributed the same for each of the materials. Because the instrument response is dependent on the source geometry (Section 4.4), the instrument efficiencies (ϵ_i) determined by placing the detectors in contact with the NIST-traceable plate sources were applicable to the measurements performed on the Oak Ridge Institute for Science and Education (ORISE) fabricated sources provided that the activity was uniformly deposited over the same active area (126 cm^2) as the NIST-traceable source. It should be noted that the preparation of a scabbled surface source by deposition on a "pre-scabbled" surface may not be representative of the actual field surface condition. That is, on a real scabbled surface the activity will likely be concentrated in the "peaks" or undisturbed surface, and will be absent in the "valleys."

5.3.2 Measurement Results for Various Surface Types

Beta measurements were performed with gas proportional and GM detectors. Two variations were used for the gas proportional detectors: detection of beta radiation only (using 3.8-mg/cm^2 window density thickness to block alpha radiation) and detection of alpha plus beta radiation. Five 1-minute measurements were made for each combination of material, geometry, and surface material. The results are presented in Table 5.4. Alpha measurements were performed with gas proportional (α-only mode) and ZnS detectors—results are presented in Table 5.5. Both alpha and beta measurements were taken at contact with the sources. The total efficiency for the point source geometry was determined by simply dividing the average net count rate by the total activity dispensed. No correction for the decay of Tc-99 or Th-230 was necessary because of their long half-lives. The total efficiency for the distributed source was determined by the following equation:

$$Total\ Efficiency = \frac{Net\ Count\ Rate}{\left(\frac{Total\ Activity}{126\ cm^2}\right) Probe\ Area} \qquad (5\text{-}1)$$

The total efficiencies determined for the distributed activity on surfaces should use the active or physical probe area, as opposed to the effective probe area, in converting instrument response to surface activity. During instrument calibration, the total efficiency is determined by placing the probe in contact with the calibration source and recording the net counts, and then dividing by the activity of the source. No correction is made for the fact that the probe has a protective screen; the total efficiency and instrument efficiency take into consideration the fact that part of the active area of the probe is covered and may be insensitive to incident radiation. Thus, surface activity measurements in the field should be corrected for the physical area of the probe, with no corrections made for the protective screen, to be consistent with the manner in which the instrument was calibrated. Refer to Section 2 for the comparison of the physical probe area and the effective probe area for each of the detectors studied.

The source efficiencies, ϵ_s, were calculated by dividing the total efficiency by the instrument efficiency. The instrument efficiencies were determined for each detector and geometry using appropriate NIST-traceable sources. As discussed in Section 4, following the ISO-7503-1 guidance for surface activity measurements requires knowledge of both the instrument and source

efficiencies. The instrument efficiency, ϵ_i, is determined during calibration using the stated 2π emission rate of the source. Source efficiencies must be experimentally determined for a given surface type and coating. Tables 5.4 and 5.5 present experimental data on source efficiencies for several common surface types. The data indicate that the source efficiency varies widely depending on the amount of self-absorption and backscatter provided by the surface. The total efficiencies may be determined from Tables 5.4 and 5.5 by simply taking the product of ϵ_i and ϵ_s.

The total efficiencies for Tc-99 and Th-230 on various surfaces determined from this experiment may be compared to the average detector efficiencies (historical calibration data from the Environmental Survey and Site Assessment Program of ORISE) presented in Table 4.2. The average Tc-99 total efficiency for a gas proportional detector operated in an alpha plus beta mode was 0.22 c/dis (on a NIST-traceable source). This study indicates that this is an appropriate total efficiency to use for untreated wood in a point source geometry (for $\alpha + \beta$ on treated wood, ϵ_i multiplied by ϵ_s equals 0.23), but may be overly conservative for stainless steel surfaces and for sealed concrete. Similarly for the Th-230, the average total efficiencies during calibration were 0.18 and 0.19 c/dis, respectively, for the ZnS and gas proportional (alpha only mode). This study indicates that for a point source geometry on untreated wood, the total efficiency is less than 50% of the historical average alpha total efficiency (0.097 and 0.061, respectively, for α-only and ZnS detectors), and for scabbled concrete, the alpha total efficiency is approximately 50 to 75% of the total efficiency obtained from historic Environmental Survey and Site Assessment Program calibration data. The effect of reduced total efficiency in the field is an increase in the survey instrumentation MDCs. Table 5.6 gives information on the MDCs for these surface types.

The minimum detectable concentrations shown in Table 5.6 reflect the differences in the source efficiency for each surface. That is, the background, counting time, and instrument efficiency were constant for each given detector and geometry. The large variations in MDC for the surface types studied should be noted. For example, using an $\alpha + \beta$ gas proportional detector to measure Tc-99 distributed over a 126-cm^2 area has an MDC range of 260 to 950 dpm/100 cm^2, depending on the surface type. However, it is the lower bound value that is typically calculated and used as the MDC (because the calibration is performed on a clean, high-backscatter reference source, with no consideration given to the actual surface measured). Furthermore, if the uncertainty in the total efficiency is incorporated into the MDC equation (refer to Equation 3-12), the MDC for finished concrete is 2,300 dpm/100 cm^2 (compared to 950 dpm/100 cm^2).

Instrument response can be affected by energy response to the source, backscatter from media, and self-absorption of radiation in the surface. It was possible that the relatively low efficiency obtained for some of the concrete surfaces was due to the penetration of the reference material into the surface and the resultant self-absorption. This porosity effect was also evident for the untreated wood
(Table 5.5). The high source efficiencies obtained on the stainless steel surface were due in part to the contribution from backscattered particles entering the detector. The backscatter contribution measured was approximately 50% for Tc-99 on stainless steel, somewhat higher than anticipated. The backscatter contribution from Tc-99 on a stainless steel surface has been estimated as 22% (NCRP 112).

The International Organization for Standardization recommends the use of factors to correct for alpha and beta self-absorption losses when determining the surface activity. Specifically, the

recommendation is to use a source efficiency of 0.5 for maximum beta energies exceeding 0.4 MeV, and to use a source efficiency of 0.25 for maximum beta energies between 0.15 and 0.4 MeV and for alpha-emitters; these values "should be used in the absence of more precisely known values" (ISO 7503-1). Although this guidance provides a starting point for selecting source efficiencies, the data in Tables 5.4 and 5.5 illustrate the need for experimentally determined source efficiencies.

In summary, both backscatter and self-absorption effects may produce considerable error in the reported surface activity levels if the field surface is composed of material significantly different in atomic number from the calibration source. Therefore, it is important to consider the effects that result when the calibration source has backscatter and self-absorption characteristics different from the field surface to be measured. The following guidance should prove beneficial when making measurements on concrete surfaces and using the conventional total efficiency to convert count data to surface activity (i.e., source efficiencies are not considered separately): use a calibration source that is mounted on an aluminum disc, since the backscatter characteristics for concrete and aluminum are similar (NCRP 112).

5.4 Attenuation Effects of Overlaying Material (Self-Absorption)

Calibration sources invariably consist of a clean, smooth surface and, as such, do not reproduce the self-absorption characteristics of surfaces in the field. Thus, the surface condition can affect the detection sensitivity of an instrument significantly, depending on the radionuclide of concern. For example, paint has a smaller impact on detection of Co-60 (beta radiation) than it does for Am-241 (alpha radiation). The effects that various surface conditions have on detection sensitivities were evaluated by depositing varying amounts of the material (i.e., water, dust, oil, paint) between the detector and the radioactive source.

5.4.1 Methodology

The effects of the following surface conditions were evaluated quantitatively: (a) dusty, (b) wet, (c) oily, and (d) painted surfaces. In order to allow intercomparison of the results from this study, it was necessary to simulate known thicknesses of materials such as dust, water, or paint on surfaces, reproducibly. Therefore, known quantities of soil (dust), water, oil, and paint were evenly spread over a surface with standard (known) dimensions to produce the desired thickness of material on the surface.

The material to be evaluated (e.g., water, dust, oil, paint) was uniformly deposited between two Mylar sheets, within the area of the Plexiglas jig. The net weight of the material was obtained and the density thickness of the material (in mg/cm^2) was calculated by dividing the weight by the area over which the material was deposited (typically 126 cm^2). It was necessary to ensure that the material was evenly spread over the active area of the Plexiglas. The following text describes how the surface coatings were prepared (oil is discussed in Section 5.4.2).

Paint

The Mylar was attached tightly to the Plexiglas jig and weighed for initial weight. A 126-cm^2 hole was cut in a piece of cardboard to match the exact active area of the 43-68 detector. The Mylar was placed beneath the cardboard jig. The paint was sprayed lightly over the surface of the Mylar at a distance that varied from 15 cm to as much as 30 cm. After the paint had dried, a new weight was obtained and subtracted from the initial weight. This yielded the test weight. After measurements were completed and the Mylar was checked for tears, the next quantity of paint was applied.

Water

A piece of Kimwipe was cut exactly to fit the active area of a 43-68 detector (126 cm^2) and placed on a new piece of Mylar. In this case, the Mylar was not stretched or attached tightly across the Mylar jig. The initial weights for the Kimwipe and Mylar sheets were then determined. A known quantity of water was then pipetted onto the Kimwipe as evenly as possible. The water was uniformly absorbed over the Kimwipe. After measurements had been performed, the Kimwipe and Mylar were folded and reweighed to measure the amount of evaporation and to determine the next test weight. Evaporation was very rapid in most cases and weight determinations had to be made following each instrument measurement series.

Dust

Dust was obtained by grinding potting soil and sieving it through 250 mesh screen. An empty plastic dish was weighed and dust was added to the dish until the desired weight was obtained. Dust was then poured onto the Mylar that was tightly stretched across the Plexiglas jig. The dish was then reweighed to obtain the exact amount of dust applied to the Mylar. The dust was spread across the Mylar to 126 cm^2. This was done by using a small (1/4-inch-wide), very fine, bristle brush. The brush was first weighed. The dust was so fine that it could not be brushed or swept, instead it was blotted until it appeared evenly distributed and within the 126-cm^2 active area of the probe. Another sheet of Mylar was placed over the dust. After the dust was distributed, the brush was again weighed to determine if any dust remained in the brush and to obtain the final test weight. This process was repeated for each test weight.

Uniformity Measurements

The uniformity of the material deposition between the Mylar sheets was evaluated by measuring the attenuation produced by the two Mylar sheets and material at five locations within the active area of the Plexiglas. Specifically, at each location, the GM detector (20-cm^2 probe area) and radioactive disc source (a low-energy beta or alpha source was used to ensure that the source was being attenuated by the material) were placed on opposite sides of the Mylar sheets. Five 1-minute measurements were obtained at each location. The measurements were averaged and the standard error in the mean was calculated at each location. Uniformity of the material was assumed to be sufficient if the relative standard error in the mean of 25 measurements (5 measurements at each locations) was less than 15%. It was recognized that exact uniformity was not practical, or even desirable, since one objective of the study was to reproduce realistic field conditions.

If the uniformity test failed, efforts continued to evenly distribute the material until the material was distributed more uniformly. Once the desired level of uniformity had been achieved, measurements were performed using the necessary detectors and calibration sources. The instrument background was determined by a series of five 1-minute counts. For each data point (i.e., combination of material, thickness, detector, and source) evaluated, five 1-minute measurements were collected (in general, the radioactive sources used in this study possessed sufficient activity to ensure that the uncertainty due to counting statistics alone was less than 5%). Each data point was statistically evaluated by calculating the mean of the gross counts and standard error in the mean of the gross counts. The background was subtracted from the mean of the gross counts, and the detector efficiency was calculated by dividing by the activity of the calibration source. The pressure and temperature in the measurement hood were recorded.

5.4.2 Measurement of Various Surface Coatings

Initially, this study was limited to performing MDC measurements with a gas proportional detector (Ludlum Model 43-68) with oil deposited between the Mylar sheets. The radioactive sources used in the pilot study were C-14, Tc-99, and SrY-90. The Tc-99 source used was a 100-cm^2 plate source; the C-14 and Sr-90 sources had 32-mm-diameter, disc-shaped geometries. The detector background for 1 minute was 326 counts. Table 5.7 presents the results of MDC measurements for each source under the following conditions: (a) detector face alone (0.4-mg/cm^2 window), (b) detector face and two sheets of Mylar (0.8-mg/cm^2, total density thickness), (c) plus 1.5 mg/cm^2 of 20W-50 motor oil (2.3-mg/cm^2, total density thickness), (d) plus 2.9 mg/cm^2 of 20W-50 motor oil (3.7-mg/cm^2, total density thickness), and (e) plus 4.5 mg/cm^2 of 20W-50 motor oil (5.3-mg/cm^2, total density thickness).

Figure 5.3 shows the effects of oil density thickness on the source efficiency. The first datum point for each source (at 0.4 mg/cm^2, not shown in figure) in Table 5.7 may be considered to yield the total efficiency under optimum laboratory conditions (smooth, clean surface). As various density thicknesses of oil were added, the source efficiency was decreased due to absorption losses. The source efficiency appeared to be reduced more significantly for the lower energy beta emitters as the density thickness of oil on the surface was increased. Figure 5.4 illustrates the effects of oil density thickness on the detector MDC (which is a function of source efficiency). The first data point for each source may be considered as the theoretical detector MDC under optimum laboratory conditions. This figure illustrates how the detector MDC, calibrated to lower energy beta emitters, was significantly affected by the oil density thickness on the surface.

This portion of the study continued with the evaluation of various thicknesses of paint, dust, and water deposited between the detector and the source. Measurements were performed with gas proportional, GM, and ZnS detectors. Three variations were used for the gas proportional detectors: (a) detection of alpha radiation only, (b) detection of beta radiation only (using 3.8-mg/cm^2 window density thickness to block alpha radiation), and (c) detection of alpha and beta radiation. The radioactive sources used in the pilot study were C-14, Tc-99, Tl-204, and SrY-90 for beta measurements, and Th-230 for alpha measurements. When measurements were performed over large area sources (i.e., 126 or 150 cm^2), the source activity within the physical area of the detector was determined. This corrected activity was used to determine total efficiencies:

$$Corrected\ Activity = \frac{(Source\ Activity)\ .\ (Probe\ Area)}{(Active\ Area\ of\ Source)} \quad (5\text{-}2)$$

Tables 5.8 through 5.28 present the results of material density thicknesses for paint, dust, and water versus source efficiency for all of the detector types evaluated. These results are consistent with the results obtained with the oil deposition. As before, the source efficiency appeared to be reduced more significantly for the lower energy beta emitters as the density thickness of the material on the surface was increased. The instrument efficiency was determined with the Mylar in place above the source for the paint and dust studies, and with the Mylar and Kimwipe sheet for the water attenuation studies. The total efficiency may be calculated for any evaluated surface coating by multiplying the instrument efficiency by the source efficiency. Figures 5.5 through 5.19 illustrate the effects of material density thicknesses on source efficiency—each figure shows the measured data and the best-fit exponential curve. Figures 5.20 to 5.23 illustrate the effects of increasing dust density thickness on the MDC calculation.

The measured source efficiency versus density thickness was fit to an exponential curve. The results of this regression fit are provided in Tables 5.8 through 5.28. The data associated with the source efficiency and density thickness were examined for the best way to present the error associated with the given measurements. It was judged that regression techniques are the best approach to describe the data as well as providing the average source efficiency and 95% confidence interval at each density thickness. The density thickness was assumed to be known without error. This is undoubtedly incorrect but, it does not affect the results significantly because the error associated in the weight measurements is small compared with the error associated with the count measurements used to determine the source efficiency. This practice is common in most regression situations and is discussed in NUREG/CR-4604, "Statistical Methods for Nuclear Material Management". The regression was used to determine the intercept and slope of the line—transformed by taking the natural logarithm—using a least-squares fit. The regression also outputs the residual mean square which is an unbiased estimator of the variance associated which the source efficiency values. Using the slope and intercept, the predicted values associated with the density thickness measurements were determined. A confidence interval was also determined using (Walpole):

$$Y_o - t_{\alpha/2}\, s\, ((1/n) + [(x_o - x)^2 / S_x])^{1/2} < Y < Y_o + t_{\alpha/2}\, s\, ((1/n) + [(x_o - x)^2 / S_x])^{1/2} \quad (5\text{-}3)$$

where,

Y_o = predicted source efficiency
$t_{\alpha/2}$ = test statistic for desired accuracy
s = sqrt of residual mean square
n = number of points in regression
x_o = density thickness of interest
x = average density thickness
$S_x = \sum (x_i - x)^2$
Y = measured source efficiency

One interesting finding was that the alpha and beta attenuation for a given radionuclide were similar, regardless of the specific material responsible for the attenuation. Figure 5.24 illustrates that the source efficiencies versus density thickness for SrY-90, Tl-204, Tc-99, and C-14 decrease fairly consistently for each of the materials tested, and may be considered independent of material type (i.e., the source efficiency decreases with increasing density thickness in the same manner for

water, dust, and paint).

The exponential term in each regression fit is a measure of the alpha or beta attenuation. That is, the exponential terms were consistent for each radionuclide—the terms ranged as follows: C-14, 0.211 to 0.291; Tc-99, 0.086 to 0.110; Tl-204, 0.031 to 0.046; SrY-90, 0.016 to 0.028; and Th-230, 0.331 to 0.906. The alpha radiation experienced the greatest variability in attenuation with different materials.

When using the fitted source efficiency data in Tables 5.8 to 5.28, it is important to note that the exponential reduction produced from a given density thickness is obtained from the exponential term alone. An example is provided to clarify the use of these data. Assume that a GM detector is calibrated to a Tc-99 point source, resulting in an ϵ_i equal to 0.278. It is determined that surface activity measurements will be performed on a concrete surface—refer to Table 5.4 to obtain ϵ_s equal to 0.630. Therefore, the total efficiency is calculated by multiplying ϵ_i by ϵ_s (equals 0.175). Now assume that there is a 2 mg/cm^2-thick coating of dust on the concrete surface—therefore, the surface efficiency (ϵ_s) must be corrected for this dust layer. Table 5.16 provides the regression equation for Tc-99 with a GM detector: $\epsilon_s = 0.669\ e^{-0.093\ x}$

To correct the surface efficiency (0.630) for the dust layer, multiply ϵ_s by the exponential term, substituting the density thickness for x: ϵ_s (for 2 mg/cm^2 dust) = (0.630) * $e^{-0.093\ (2)}$ = 0.523.

Now the total efficiency for this condition becomes $\epsilon_{tot} = \epsilon_i * \epsilon_s$ = (0.278) (0.523) = 0.146, as compared to 0.175 without consideration of the dust layer.

5.5 Use of Alpha and/or Beta Measurements to Assess Surface Activity

The uranium and thorium decay series emit both alpha and beta radiation. A common practice has been to use beta measurements to demonstrate compliance with those surface activity guidelines expressed as alpha activity. In the case of uranium, the current surface activity guidelines are specified in alpha disintegrations per minute—e.g., 5,000 α dpm/100 cm^2. When applying beta measurements to assess compliance with uranium and thorium surface activity guidelines, consideration should be given to the radionuclide (specifically the energy of the radionuclide) used to calibrate the detector. For example, SrY-90, a high energy beta-emitter, is often used to calibrate a detector for surface activity measurements of uranium. That is, a SrY-90 calibration source is assumed to be sufficiently representative of the beta emissions from the uranium surface contamination and, therefore, it is assumed that the total efficiency using a SrY-90 source will provide an adequate representation of the uranium contamination. An experiment was designed to evaluate the agreement between total efficiencies obtained from a SrY-90 source and processed uranium contamination. Additionally, an experiment was performed with 3% enriched uranium (3% of U-235 by weight) to assess the applicability of calculating the total efficiency for uranium by considering the detector's response to each of the alpha and beta emissions in the decay series.

For these experiments, known quantities of NIST-traceable SrY-90, Ru-106 (Rh-106), processed uranium, and 3% enriched uranium (in aqueous solutions), were dispensed on various surface materials (i.e., stainless steel, concrete, wood and drywall). Processed uranium includes U-238

that is in equilibrium with U-234, but with the remaining decay series radionuclides removed; and U-235 is present at the natural isotopic ratio (0.7% of U-235 by weight). The 3% enriched uranium exhibited a U-234-to-U-235 ratio of 24, and had the following alpha activity fractions: 0.167, U-238; 0.033, U-235; and 0.799, U-234. For each surface material, SrY-90, Ru-106 (Rh-106), and uranium were dispensed to simulate a small, disc-source geometry—the areal extent of the source activity was less than 20 cm^2. The total SrY-90 activity dispensed was 5,229 dpm and approximately 4,200 dpm for the Ru-106 (Rh-106). The total processed uranium activity was 7,840 alpha dpm—approximately comprised of 3,900 dpm U-238; 3,760 dpm U-234; and 180 dpm U-235. The amount of enriched uranium dispensed was 4,520 dpm; uranium isotopic fractions can be calculated using the alpha activity fractions provided above. Once dispensed, the radioactivity was allowed to dry overnight in a ventilated hood.

Background count rates were obtained for instrument/surface combinations that were used to make surface activity measurements of the deposited activity. Beta measurements were performed with gas proportional and GM detectors. As before, two variations were used for the gas proportional detectors, including detection of beta radiation only (using 3.8 mg/cm^2 window density thickness to absorb alpha radiation) and detection of alpha plus beta radiation. Alpha measurements were performed with gas proportional (alpha only mode) and ZnS detectors. Five, 1-minute measurements were performed for each source and surface material combination. Total efficiencies were calculated by dividing the net count rate by the activity dispensed on the particular surface. For uranium, the total alpha activity was used to determine the total efficiencies. Results are presented in Table 5.29.

The first observation that can be made is that the alpha efficiencies for the α-only gas proportional and ZnS detectors are low as compared to the historical efficiencies obtained from ESSAP electroplated calibration sources (refer to Table 4.2). One possible reason for this reduction in alpha efficiency is that the liquid sources were allowed to air dry—and as such, the resulting source deposition did not constitute a "weightless" source (i.e. source with virtually no self-absorption). That is, the uranium source deposition was probably responsible for measurable self-absorption of the alpha radiation. It should be noted that while experimental controls could have been exercised to make the uranium source deposition approximately "weightless," the actual source deposition used is likely more realistic to the uranium contamination measured in the field.

The second observation made was that the SrY-90 source, deposited on stainless steel and concrete surfaces, exhibited total efficiencies for the alpha plus beta gas proportional and GM detectors very similar to those of processed uranium. The total efficiency for SrY-90 with the beta-only gas proportional detector was about 50% higher than the processed uranium total efficiency (i.e., 0.38 c/dis versus 0.24 c/dis on stainless steel). Therefore, the assessment of uranium contamination using a beta-only gas proportional detector calibrated to SrY-90 would result in an underestimate of the surface activity. An explanation for the difference is provided. The alpha plus beta gas proportional and GM detector's response to processed uranium includes a measurable component due to the alpha radiation. Specifically, the detector is responding to a variety of radiations from the processed uranium—including alpha radiation from the three isotopes of uranium and beta radiations from the progeny of U-238 and U-235—and the total efficiency is only related to the total alpha activity of the uranium. Therefore, the total efficiency

based on the alpha activity of processed uranium is similar to the efficiency of these detectors (alpha plus beta gas proportional and GM) calibrated to SrY-90. In the case of the beta-only gas proportional detector, the response to alpha radiation has been nearly eliminated through the use of the 3.8-mg/cm^2 window, and the resulting detector response to the beta component of processed uranium is much less than that of SrY-90 (a subsequent example will illustrate the components of the detector response to uranium). However, consistent with the scope of this document, the total efficiency for processed uranium should be considered under field conditions. That is, while there is agreement between the total efficiencies for SrY-90 and the processed uranium under ideal laboratory conditions, field conditions may affect the detector's response to these materials to varying degrees.

To evaluate the potential effect of overlaying material in the field, thin sheets of Mylar were placed over the processed uranium deposited on stainless steel. Five, 1-minute measurements were performed for each Mylar thickness and detector combination. The total efficiencies were calculated by dividing the net count rate by the activity dispensed on the particular surface, and the results were normalized to the total efficiency obtained with no Mylar. Results are presented in Table 5.30. As expected, the total efficiency for the alpha detectors exhibited a significant reduction for the range of Mylar thicknesses evaluated (0.22 to 3.30 mg/cm^2). Conversely, the detectors that respond primarily to beta radiation experienced only a modest reduction in total efficiency. Because a large fraction of the detector's response to processed uranium is due to the high-energy Pa-234m beta radiation, the addition of absorber sheets serves to primarily attenuate the lower energy beta radiation and alpha radiation associated with uranium. For comparison, the attenuation effects of overlaying material over this thickness range for SrY-90, discussed in Section 5.4 and illustrated in the corresponding tables, shows a normalized total efficiency of approximately 0.90 for 3.30 mg/cm^2 of Mylar (compared to 0.76 and 0.80 for the alpha plus beta and GM detectors, respectively, for processed uranium). Therefore, depending on the expected field conditions, the use of a SrY-90 calibration source for processed uranium may slightly underestimate the surface activity using alpha plus beta gas proportional and GM detectors. It is expected that only a minor correction (reduction in SrY-90 determined efficiency) would be necessary for field conditions because most of the response is from the high-energy beta.

As discussed previously, using the beta-only gas proportional detector calibrated to SrY-90 would result in an underestimate of the processed uranium surface activity, because of the comparison of total efficiencies (i.e., 0.38 c/dis for SrY-90 versus 0.24 c/dis for processed uranium). However, as Table 5.30 indicates, the total efficiency for the beta-only gas proportional detector is largely insensitive to the range of absorber thicknesses used to assess detector response under field conditions. Therefore, it may be desirable to use this detector for the assessment of processed uranium contamination using a detector calibrated to an appropriate beta energy (to yield about 24% total efficiency). Table 4.2 indicates that an appropriate beta energy may be Tl-204, or a radionuclide with a slightly less average beta energy.

The total efficiencies for the 3% enriched uranium were less than those for processed uranium, because of the increased alpha activity fraction from U-234 (Table 5.29). The determination of an appropriate beta calibration energy is more difficult than for processed uranium because of the increase in alpha activity. The most representative calibration source would be one prepared from the radioactive material (e.g., uranium or thorium) that is being measured in the field. Because many detectors used for surface activity assessment can respond to alpha and beta radiations to

varying degrees, using a single radionuclide (or even one in equilibrium with another radionuclide, SrY-90) for calibration may not be representative of the complex decay scheme of uranium and thorium decay series. In this situation, it may be more appropriate to determine the total efficiency by considering the detector's response to each of the alpha and beta emissions in the decay series. An example of this approach is discussed for 3% enriched uranium on stainless steel.

In order to evaluate the detector's response to each of the alpha and beta emissions in the decay of low enriched uranium, the decay scheme of the contamination must be completely understood in terms of radiation type, energy, and abundance. Table 5.31 illustrates the total efficiency calculation for 3% low enriched uranium, as measured by a 126-cm^2 alpha plus beta gas proportional detector. The alpha fractions of U-238, U-235 and U-234 were determined for 3% enriched uranium and the detector's total efficiency (4π) for each radiation emission was determined by experiment and/or empirical relationship. For example, the detector's response to the alpha emissions of U-238, U-235, and U-234 were assessed experimentally with Th-230 and Pu-239 calibration sources, the Th-231 beta energies from the U-235 series were determined using a Tc-99 calibration source. Beta energies that could not be determined via experiment due to the lack of an appropriate beta calibration standard, were calculated empirically. In this regard, the beta efficiency for Ru-106 (Rh-106) was determined to assist with the appropriate efficiency for the Pa-234m. As shown in Table 4.2, the total efficiency for SrY-90 (average beta energy of 563 keV) is about 0.42, while the total efficiency for Ru-106 (average beta from Rh-106 is 1410 keV) on stainless steel is 0.57; therefore, it was possible to determine the total efficiency for Pa-234m (819 keV average beta energy) using these data. The total weighted efficiency for 3% enriched uranium was 0.257—which compares favorably to the measured total efficiency of 0.23.

Using this approach, it is possible to assess the fractional detector response from each radionuclide in the decay series. In this example, about 33% of the gas proportional detector's response is due to the high energy beta of Pa-234m, while nearly 60% is from the alpha activity. Therefore, the 25.7% total efficiency calculated should be considered as the ideal laboratory efficiency, and should be corrected for expected field conditions. For example, each of the individual radionuclide total efficiencies could be corrected for field conditions using the exponential reduction discussed in Section 5.4.

Alternatively, the same approach illustrated in Table 5.31 could be performed for the beta-only detector—which has the advantage of not being as sensitive to field conditions as are the detectors that respond to alpha radiation. This approach was performed and the resulting total efficiency was 0.096 (Table 5.32). The measured total efficiency (0.09) compared favorably. Most of the response (about 80%) is from the high energy beta of Pa-234m, which is not likely to be attenuated to a significant degree. It should be noted that this calculational technique is detector-dependent—i.e., the specific detector's response to various radiations must be carefully assessed.

Table 5.1 Background Count Rate for Various Materials

Surface Material	Background Count Rate (cpm)[a]					
	Gas Proportional			GM	ZnS	NaI
	α Only	ß Only	α + ß			
Ambient[b]	1.00 ± 0.45[c]	349 ± 12	331.6 ± 6.0	47.6 ± 2.6	1.00 ± 0.32	4702 ± 16
Brick	6.00 ± 0.84	567.2 ± 7.0	573.2 ± 6.4	81.8 ± 2.3	1.80 ± 0.73	5167 ± 23
Ceramic Block	15.0 ± 1.1	792 ± 11	770.2 ± 6.4	107.6 ± 3.8	8.0 ± 1.1	5657 ± 38
Ceramic Tile	12.6 ± 0.24	647 ± 14	648 ± 16	100.8 ± 2.7	7.20 ± 0.66	4649 ± 37
Concrete Block	2.60 ± 0.81	344.0 ± 6.2	325.0 ± 6.0	52.0 ± 2.5	1.80 ± 0.49	4733 ± 27
Drywall	2.60 ± 0.75	325.2 ± 8.0	301.8 ± 7.0	40.4 ± 3.0	2.40 ± 0.24	4436 ± 38
Floor Tile	4.00 ± 0.71	308.4 ± 6.2	296.6 ± 6.4	43.2 ± 3.6	2.20 ± 0.58	4710 ± 13
Linoleum	2.60 ± 0.98	346.0 ± 8.3	335.4 ± 7.5	51.2 ± 2.8	1.00 ± 0.45	4751 ± 27
Carbon Steel	2.40 ± 0.68	322.6 ± 8.7	303.4 ± 3.4	47.2 ± 3.3	1.00 ± 0.54	4248 ± 38
Treated Wood	0.80 ± 0.37	319.4 ± 8.7	295.2 ± 7.9	37.6 ± 1.7	1.20 ± 0.20	4714 ± 40
Untreated Wood	1.20 ± 0.37	338.6 ± 9.4	279.0 ± 5.7	44.6 ± 2.9	1.40 ± 0.51	4623 ± 34

[a]Background count rates determined from the mean of five 1-minute counts.
[b]Ambient background determined at the same location as for all measurements, but without the surface material present.
[c]Uncertainties represent the standard error in the mean count rate, based only on counting statistics.

Table 5.2 Minimum Detectable Concentrations for Various Materials

Surface Material	Minimum Detectable Concentration (dpm/100 cpm^2)[a]	
	Gas Proportional	
	α Only	ß Only
Ambient	30	285
Brick	57	361
Ceramic Block	83	425
Ceramic Tile	78	385
Concrete Block	41	283
Drywall	41	275
Floor Tile	49	268
Linoleum	41	284
Steel	40	275
Treated Wood	28	273
Untreated Wood	32	281

[a]MDCs were calculated based on the background count rates presented in Table 5.1 for the gas proportional detector. The alpha only and beta only efficiencies were assumed to be 0.20 and 0.25 count per disintegration, respectively. Probe area corrections of 126 cm^2 were made for the gas proportional detectors. The following MDC equation was used for 1-minute counts:

$$MDC = \frac{3 + 4.65\sqrt{C_B}}{KT}$$

Table 5.3 Efficiencies and Backscatter Factors for SrY-90

Surface Material	Gas Proportional Detector With 0.4-mg/cm^2 Window		Gas Proportional Detector With 3.8-mg/cm^2 Window	
	Total Efficiency[a] (c/dis)	Backscatter Factor[b]	Total Efficiency (c/dis)	Backscatter Factor
Air	0.28	1.00	0.25	1.00
Wood	0.34	1.20	0.29	1.14
Stainless Steel	0.40	1.43	0.35	1.37
Drywall	0.35	1.24	0.28	1.11
Carbon Steel	0.40	1.42	0.33	1.32
Floor Tile	0.35	1.25	0.31	1.23
Sealed Concrete	0.37	1.30	0.31	1.22
Concrete Block	0.35	1.25	0.31	1.22

[a]Total efficiency was determined by dividing the instrument net counts by the deposited SrY-90 activity.
[b]The backscatter factor was calculated by dividing the particular surface material efficiency by the efficiency in the air.

Table 5.4 Surface Material Effects on Source Efficiency for Tc-99 Distributed on Various Surfaces

Surface Material	Source Efficiency[a,b]		
	Gas Proportional		GM
	β Only	α + β	
Point Source[c]			
Sealed Concrete[d]	0.703 ± 0.079[e]	0.694 ± 0.063	0.630 ± 0.076
Stainless Steel	0.755 ± 0.096	0.761 ± 0.076	0.773 ± 0.091
Untreated Wood	0.53 ± 0.11	0.504 ± 0.053	0.512 ± 0.061
Distributed Source[f]			
Sealed Concrete	0.299 ± 0.096	0.20 ± 0.12	0.19 ± 0.18
Stainless Steel	0.81 ± 0.13	0.73 ± 0.11	---[g]
Treated Wood	0.66 ± 0.11	0.551 ± 0.088	0.61 ± 0.52

[a]Source efficiency determined by dividing the total efficiency by the instrument efficiency.
[b]The instrument efficiencies for the point source geometry were 0.25, 0.45, and 0.28, respectively, for the β only, α + β, and GM detectors. Instrument efficiencies for the distributed source geometry were 0.20, 0.38, and 0.20, respectively, for the β only, α + β, and GM detectors.
[c]The Tc-99 activity (2828 ± 91 dpm) was dispensed over an area less than 5 cm^2.
[d]For sealed concrete, the Tc-99 activity (5,660 ± 110 dpm) was dispensed over an area of approximately 4 cm^2.
[e]Uncertainties represent the 95% confidence interval, based on propagating the errors in pipetting, volumetric measurements, calibration source activity, and in counting statistics.
[f]The Tc-99 activity (2830 ± 100 dpm) was evenly distributed over an area of 126 cm^2.
[g]Measurement not performed.

Table 5.5 Surface Material Effects on Source Efficiency for Th-230 Distributed onVarious Surfaces

Surface Material	Source Efficiency[a,b]	
	Gas Proportional (α only)	ZnS
Point Source[c]		
Scabbled Concrete	0.276 ± 0.013[d]	0.288 ± 0.026
Stainless Steel	0.499 ± 0.028	0.555 ± 0.043
Untreated Wood	0.194 ± 0.023	0.185 ± 0.025
Distributed Source[e]		
Sealed Concrete	0.473 ± 0.053	0.428 ± 0.054
Carbon Steel	0.250 ± 0.042	0.216 ± 0.031
Treated Wood	0.527 ± 0.057	0.539 ± 0.065

[a]Source efficiency determined by dividing the total efficiency by the instrument efficiency.
[b]The instrument efficiencies for the point source geometry were 0.50 and 0.33, respectively, for the α-only and ZnS detectors. Instrument efficiencies for the distributed source geometry were 0.40 and 0.31, respectively, for the α-only and ZnS detectors.
[c]The Th-230 activity (4,595 ± 79 dpm) was dispensed over an area less than 10 cm^2.
[d]Uncertainties represent the 95% confidence interval, based on propagating the errors in pipetting, volumetric measurements, calibration source activity, and in counting statistics.
[e]The Th-230 activity (4,600 ± 170 dpm) was evenly distributed over an area of 126 cm^2.

Table 5.6 Surface Material Effects on MDC for Tc-99 and Th-230 Distributed on Various Surfaces

Surface Material	Minimum Detectable Concentration[a] (dpm/100 cm^2)				
	Tc-99			Th-230	
	α + β	β only	GM	α only	ZnS
Point Source[b]					
Sealed Concrete	242 ± 13[c]	396 ± 46	1,090 ± 180	---	---
Scabbled Concrete	---	---	---	88 ± 16	131 ± 89
Stainless Steel	192 ± 19	359 ± 47	850 ± 130	32 ± 13	68 ± 28
Untreated Wood	285 ± 31	520 ± 110	1,200 ± 150	67 ± 30	190 ± 100
Distributed Source[d]					
Sealed Concrete	950 ± 560	1,220 ± 380	5,100 ± 4,800	37 ± 23	84 ± 40
Stainless Steel	260 ± 34	446 ± 64	---	---	---
Treated Wood	312 ± 44	523 ± 79	1,500 ± 1300	27.1 ± 7.7	64.8 ± 9.8
Carbon Steel	---	---	---	81 ± 21	153 ± 54

[a]The minimum detectable concentration was calculated using 1-minute counts and total efficiencies determined on the basis of the known amount of activity deposited.
[b]The point (disc) source area for Tc-99 and Th-230 were approximately 5 and 10 cm ^{2}, respectively.
[c]Uncertainties represent the 95% confidence interval, based on propagating the errors in pipetting, volumetric measurements, calibration source activity, and in counting statistics.
[d]The distributed source area for both Tc-99 and Th-230 was 126 cm ^{2}.

Table 5.7 Effects of Oil Density Thickness on Source Efficiency and MDC (Gas Proportional—α + β)

Surface Material	Density Thickness (mg/cm²)	C-14 (0.254)[a]		Tc-99 (0.364)		SrY-90 (0.536)	
		Source Efficiency[b]	MDC[c] (dpm/100 cm²)	Source Efficiency	MDC (dpm/100 cm²)	Source Efficiency	MDC (dpm/100 cm²)
Detector Face[d]	0.4	NA	605	NA	304	NA	164
Detector Face[e] Plus 2 Sheets Mylar	0.8	0.386	703	0.596	317	0.772	167
Plus 1.5 mg/cm² Oil[f]	2.3	0.236	1,148	0.467	406	0.744	173
Plus 2.9 mg/cm² Oil	3.7	0.193	1,406	0.401	472	0.700	184
Plus 4.5 mg/cm² Oil	5.3	0.102	2,651	0.349	543	0.677	190

[a]Instrument efficiency provided in parentheses.
[b]Source efficiency was determined by dividing the total efficiency by the instrument efficiency.
[c]Probe area corrections of 126 cm² were made for the gas proportional detectors. The following MDC equation was used for 1-minute counts and a background of 326 cpm:

$$MDC = \frac{3 + 4.65\sqrt{C_B}}{KT}$$

[d]Measurements performed with a Ludlum 43-68 gas proportional detector with a standard 0.4 mg/cm² window.
[e]Each sheet of Mylar has a density thickness of 0.22 mg/cm².
[f]20W-50 motor oil used for study.

Table 5.8 Effects of Paint Density Thickness on Source Efficiency and MDC (Gas Proportional— α + β)

Surface Material	Density Thickness (mg/cm^2)	C-14 (0.254 ± 0.006)[a]			Tc-99 (0.364 ± 0.029)			Tl-204 (0.450 ± 0.025)			SrY-90 (0.537 ± 0.027)		
		Source Efficiency		MDC[d] (dpm/100 cm^2)	Source Efficiency		MDC (dpm/100 cm^2)	Source Efficiency		MDC (dpm/100 cm^2)	Source Efficiency		MDC (dpm/100 cm^2)
		Meas.[b]	Fit[c]		Meas.	Fit		Meas.	Fit		Meas.	Fit	
Detector Face[e]	0.4	NA	NA	510	NA	NA	278	NA	NA	202	NA	NA	177
Detector Face[f] Plus 2 Sheets Mylar	0.84	0.437	0.426 ± 0.065	600	0.626	0.572 ± 0.100	291	0.716	0.675 ± 0.079	206	0.697	0.643 ± 0.103	178
Plus 1.93 mg/cm^2 Paint[g]	2.77	0.252	0.243 ± 0.030	1,037	0.427	0.463 ± 0.066	427	0.596	0.622 ± 0.060	247	0.584	0.615 ± 0.080	212
Plus 2.48 mg/cm^2 Paint	3.32	0.215	0.207 ± 0.024	1,215	---[h]	---	---	---	---	---	---	---	---
Plus 5.54 mg/cm^2 Paint	6.38	0.074	0.085 ± 0.008	3,542	0.300	0.311 ± 0.034	608	0.515	0.535 ± 0.039	286	0.530	0.565 ± 0.056	233
Plus 9.48 mg/cm^2 Paint	10.32	0.026	0.027 ± 0.004	9,955	0.201	0.202 ± 0.027	907	0.449	0.454 ± 0.042	329	0.513	0.515 ± 0.064	241
Plus 12.63 mg/cm^2 Paint	13.47	0.012	0.011 ± 0.002	22,593	0.147	0.143 ± 0.027	1,238	0.410	0.398 ± 0.051	360	0.498	0.479 ± 0.083	249
Regression Equation		$\epsilon_s = 0.544\ e^{-0.291 x}$			$\epsilon_s = 0.628\ e^{-0.110 x}$			$\epsilon_s = 0.699\ e^{-0.042 x}$			$\epsilon_s = 0.656\ e^{-0.023 x}$		

[a]Instrument efficiency provided in parentheses; uncertainties represent the 95% confidence interval.
[b]Source efficiency was determined by dividing the total efficiency by the instrument efficiency.
[c]The measured source efficiency versus density thickness was fit to an exponential curve; uncertainties represent the 95% confidence interval.
[d]Probe area corrections of 126 cm^2 were made for the gas proportional detectors. The following MDC equation was used for 1-minute counts and a background of 301 cpm:

$$MDC = \frac{3 + 4.65\sqrt{C_B}}{KT}$$

[e]Measurements performed with a Ludlum 43-68 gas proportional detector with a standard 0.4 mg/cm^2 window.
[f]Each sheet of Mylar has a density thickness of 0.22 mg/cm^2.
[g]Orange fluorescent waterbase paint.
[h]Measurement not performed.

Table 5.9 Effects of Paint Density Thickness on Source Efficiency and MDC (Gas Proportional—α-Only)

Surface Material	Density Thickness (mg/cm^2)	Th-230 (0.349 ± 0.015)[a]		
		Source Efficiency		MDC[d] (dpm/100 cm^2)
		Meas.[b]	Fit[c]	
Detector Face[e]	0.4	NA	NA	30
Detector Face[f] plus 2 Sheets of Mylar	0.84	0.509	0.513 ± 0.085	34
Plus 1.93 mg/cm^2 Paint[g]	2.77	0.129	0.123 ± 0.013	135
Plus 2.48 mg/cm^2 Paint	3.32	0.078	0.082 ± 0.009	223
Plus 5.54 mg/cm^2 Paint	6.38	0.008	0.008 ± 0.002	2,060
Plus 9.48 mg/cm^2 Paint	10.32[h]	0.001	NA	17,369
Regression Equation		$\epsilon_s = 0.956\ e^{-0.741\ x}$		

[a]Instrument efficiency provided in parentheses; uncertainties represent the 95% confidence interval.
[b]Source efficiency was determined by dividing the total efficiency by the instrument efficiency.
[c]The measured source efficiency versus density thickness was fit to an exponential curve; uncertainties represent the 95% confidence interval.
[d]Probe area corrections of 126 cm^2 were made for the gas proportional detectors. The following MDC equation was used for 1-minute counts and a background of 1 cpm:

$$MDC = \frac{3 + 4.65\sqrt{C_B}}{KT}$$

[e]Measurements performed with a Ludlum 43-68 gas proportional detector with a standard 0.4-mg/cm^2 window.
[f]Each sheet of Mylar has a density thickness of 0.22 mg/cm^2.
[g]Orange fluorescent waterbase paint.
[h]Data point not used in regression fit due to limited alpha range.

Table 5.10 Effects of Paint Density Thickness on Source Efficiency and MDC (Gas Proportional—β-Only)

Surface Material	Density Thickness (mg/cm²)	C-14 (0.081 ± 0.002)[a]			Tc-99 (0.191 ± 0.016)			Tl-204 (0.355 ± 0.021)			SrY-90 (0.465 ± 0.024)		
		Source Efficiency		MDC[d] (dpm/100 cm²)	Source Efficiency		MDC (dpm/100 cm²)	Source Efficiency		MDC (dpm/100 cm²)	Source Efficiency		MDC (dpm/100 cm²)
		Meas.[b]	Fit[c]		Meas.	Fit		Meas.	Fit		Meas.	Fit	
Detector Face[e]	3.8	NA	NA	1,823	NA	NA	577	N/A	NA	280	NA	NA	222
Detector Face[f] Plus 2 Sheets Mylar	4.24	0.435	0.445 ± 0.055	2,039	0.628	0.625 ± 0.008	599	0.715	0.707 ± 0.040	283	0.696	0.691 ± 0.021	222
Plus 1.93 mg/cm² Paint[g]	6.17	0.269	0.255 ± 0.026	3,296	0.521	0.522 ± 0.005	722	0.657	0.663 ± 0.030	308	0.669	0.669 ± 0.017	231
Plus 2.48 mg/cm² Paint	6.72	0.228	0.217 ± 0.021	3,882	---[h]	---	---	---	---	---	---	---	---
Plus 5.54 mg/cm² Paint	9.78	0.081	0.090 ± 0.007	10,893	0.370	0.373 ± 0.003	1,105	0.592	0.588 ± 0.021	342	0.627	0.631 ± 0.012	246
Plus 9.48 mg/cm² Paint	13.72	0.028	0.029 ± 0.003	31,920	0.259	0.258 ± 0.002	1,450	0.499	0.516 ± 0.023	405	0.583	0.592 ± 0.014	265
Plus 12.63 mg/cm² Paint	16.87	0.012	0.012 ± 0.002	72,542	0.192	0.192 ± 0.003	1,958	0.475	0.465 ± 0.028	426	0.570	0.562 ± 0.019	271
Regression Equation		$\epsilon_s = 1.51\ e^{-0.289\ x}$			$\epsilon_s = 0.929\ e^{-0.093\ x}$			$\epsilon_s = 0.813\ e^{-0.033\ x}$			$\epsilon_s = 0.740\ e^{-0.016\ x}$		

[a] Instrument efficiency provided in parentheses; uncertainties represent the 95% confidence interval.
[b] Source efficiency was determined by dividing the total efficiency by the instrument efficiency.
[c] The measured source efficiency versus density thickness was fit to an exponential curve; uncertainties represent the 95% confidence interval.
[d] Probe area corrections of 126 cm² were made for the gas proportional detectors. The following MDC equation was used for 1-minute counts and a background of 354 cpm:

$$MDC = \frac{3 + 4.65\sqrt{C_B}}{KT}$$

[e] Measurements performed with a Ludlum 43-68 gas proportional detector with a standard alpha-blocking 3.8-mg/cm² window.
[f] Each sheet of Mylar has a density thickness of 0.22 mg/cm².
[g] Orange fluorescent water base paint.
[h] Measurement not performed.

Table 5.11 Effects of Paint Density Thickness on Source Efficiency and MDC (GM Detector)

Surface Material	Density Thickness (mg/cm^2)	C-14 (0.099 ± 0.002)[a]			Tc-99 (0.193 ± 0.021)			Tl-204 (0.278 ± 0.017)			SrY-90 (0.388 ± 0.020)		
		Source Efficiency		MDC[d] (dpm/100 cm^2)	Source Efficiency		MDC (dpm/100 cm^2)	Source Efficiency		MDC (dpm/100 cm^2)	Source Efficiency		MDC (dpm/100 cm^2)
		Meas.[b]	Fit[c]		Meas.	Fit		Meas.	Fit		Meas.	Fit	
Detector Face[e]	---[f]	NA	NA	3,757	NA	NA	1,454	NA	NA	888	NA	NA	648
Detector Face[g] Plus 2 Sheets of Mylar	0.44	0.436	0.465 ± 0.050	4,098	0.627	0.646 ± 0.061	1,468	0.716	0.712 ± 0.028	894	0.697	0.681 ± 0.056	657
Plus 1.93 mg/cm^2 Paint[h]	2.37	0.284	0.266 ± 0.023	6,294	0.527	0.530 ± 0.041	1,748	0.671	0.670 ± 0.021	952	0.666	0.660 ± 0.044	688
Plus 2.48 mg/cm^2 Paint	2.92	0.239	0.227 ± 0.019	7,485	---[i]	---	---	---	---	---	---	---	---
Plus 5.54 mg/cm^2 Paint	5.98	0.089	0.094 ± 0.007	20,012	0.388	0.366 ± 0.022	2,373	0.599	0.599 ± 0.015	1,068	0.594	0.622 ± 0.032	771
Plus 9.48 mg/cm^2 Paint	9.92	0.029	0.030 ± 0.003	61,664	0.245	0.244 ± 0.018	3,767	0.517	0.529 ± 0.016	1,238	0.575	0.584 ± 0.038	797
Plus 12.63 mg/cm^2 Paint	13.07	0.012	0.012 ± 0.002	145,037	0.172	0.177 ± 0.018	5,362	0.487	0.479 ± 0.020	1,312	0.571	0.554 ± 0.050	802
Regression Equation		$\epsilon_s = 0.528\ e^{-0.289\ x}$			$\epsilon_s = 0.676\ e^{-0.103\ x}$			$\epsilon_s = 0.722\ e^{-0.031\ x}$			$\epsilon_s = 0.686\ e^{-0.016\ x}$		

[a] Instrument efficiency provided in parentheses; uncertainties represent the 95% confidence interval.
[b] Source efficiency was determined by dividing the total efficiency by the instrument efficiency.
[c] The measured source efficiency versus density thickness was fit to an exponential curve; uncertainties represent the 95% confidence interval.
[d] The following MDC equation was used for 1-minute counts, with a background of 49 cpm and a probe area of 20 cm^2:

$$MDC = \frac{3 + 4.65\sqrt{C_B}}{KT}$$

[e] Measurements performed with an Eberline HP - 260 GM detector with a standard mica window, typical thickness 1.4 to 2.0 mg/cm^2.
[f] Detector face is fixed part of detector and is not removable.
[g] Each sheet of Mylar has a density thickness of 0.22 mg/cm^2.
[h] Orange fluorescent water base paint.
[i] Measurement not performed.

Table 5.12 Effects of Paint Density Thickness on Source Efficiency and MDC (ZnS Scintillation Detector)

Surface Material	Density Thickness (mg/cm^2)	Th-230 (0.259 ± 0.013)[a]		
		Source Efficiency		MDC[d] (dpm/100 cm^2)
		Meas.[b]	Fit[c]	
Detector Face[e]	---[f]	NA	NA	65
Detector Face[g] Plus 2 Sheets of Mylar	0.44	0.509	0.523 ± 0.125	294
Plus 1.93 mg/cm^2 Paint[h]	2.37	0.099	0.091 ± 0.014	404
Plus 2.48 mg/cm^2 Paint	2.92	0.053	0.055 ± 0.008	756
Plus 5.54 mg/cm^2 Paint	5.98	0.003	0.004 ± 0.001	11,619
Plus 9.48 mg/cm^2 Paint	9.92[i]	0.001	NA	67,400
Regression Equation		$\epsilon_s = 0.779\ e^{-0.906\ x}$		

[a]Instrument efficiency provided in parentheses; uncertainties represent the 95% confidence interval.
[b]Source efficiency was determined by dividing the total efficiency by the instrument efficiency.
[c]The measured source efficiency versus density thickness was fit to an exponential curve; uncertainties represent the 95% confidence interval.
[d]The following MDC equation was used for 1-minute counts, with a background of 1 cpm and a probe area of 74 cm^2:

$$MDC = \frac{3 + 4.65\sqrt{C_B}}{KT}$$

[e]Measurements performed with an Eberline AC3-7 ZnS scintillation detector with a standard 1.5-mg/cm^2 window.
[f]Detector face is fixed part of detector and is not removable.
[g]Each sheet of Mylar has a density thickness of 0.22 mg/cm^2.
[h]Orange fluorescent waterbase paint.
[i]Data point not used in regression fit due to limited alpha range.

Table 5.13 Effects of Dust Density Thickness on Source Efficiency and MDC (Gas Proportional—α + β)

Surface Material	Density Thickness (mg/cm²)	C-14 (0.254 ± 0.006)[a]			Tc-99 (0.364 ± 0.029)			Tl-204 (0.450 ± 0.025)			SrY-90 (0.537 ± 0.027)		
		Source Efficiency		MDC[d] (dpm/100 cm²)	Source Efficiency		MDC (dpm/100 cm²)	Source Efficiency		MDC (dpm/100 cm²)	Source Efficiency		MDC (dpm/100 cm²)
		Meas.[b]	Fit[c]		Meas.	Fit		Meas.	Fit		Meas.	Fit	
Detector Face[e]	0.4	NA	NA	510	NA	NA	278	NA	NA	202	NA	NA	177
Detector Face[f] plus 2 Sheets of Mylar	0.84	0.437	0.432 ± 0.148	599	0.626	0.592 ± 0.086	292	0.716	0.706 ± 0.037	206	0.697	0.691 ± 0.031	178
Plus 2.28 mg/cm² Dust[c]	3.12	0.218	0.265 ± 0.064	1,201	0.425	0.465 ± 0.045	430	0.620	0.636 ± 0.024	238	0.642	0.649 ± 0.021	193
Plus 4.11 mg/cm² Dust	4.95	0.205	0.179 ± 0.035	1,276	0.407	0.383 ± 0.032	449	0.595	0.585 ± 0.018	248	0.616	0.617 ± 0.016	201
Plus 6.10 mg/cm² Dust	6.94	0.142	0.116 ± 0.023	1,847	0.297	0.310 ± 0.026	614	0.536	0.534 ± 0.016	275	0.594	0.583 ± 0.015	208
Plus 7.99 mg/cm² Dust	8.83	0.071	0.078 ± 0.019	3,675	0.245	0.253 ± 0.027	745	0.474	0.490 ± 0.019	311	0.536	0.553 ± 0.018	231
Plus 9.99 mg/cm² Dust	10.83	0.047	0.050 ± 0.017	5,534	0.215	0.205 ± 0.029	848	0.456	0.447 ± 0.023	323	0.532	0.523 ± 0.023	233
Regression Equation		$\epsilon_s = 0.518\ e^{-0.215\ x}$			$\epsilon_s = 0.647\ e^{-0.106\ x}$			$\epsilon_s = 0.733\ e^{-0.046\ x}$			$\epsilon_s = 0.708\ e^{-0.028\ x}$		

[a]Instrument efficiency provided in parentheses; uncertainties represent the 95% confidence interval.
[b]Source efficiency was determined by dividing the total efficiency by the instrument efficiency.
[c]The measured source efficiency versus density thickness was fit to an exponential curve; uncertainties represent the 95% confidence interval.
[d]Probe area corrections of 126 cm² were made for the gas proportional detectors. The following MDC equation was used for 1-minute counts and a background of 301 cpm:

$$MDC = \frac{3 + 4.65\sqrt{C_B}}{KT}$$

[e]Measurements performed with a Ludlum 43-68 gas proportional detector with a standard 0.4-mg/cm² window.
[f]Each sheet of Mylar has a density thickness of 0.22 mg/cm².
[g]Dust obtained by grinding potting soil and sieving through 250 mesh screen.

Table 5.14 Effects of Dust Density Thickness on Source Efficiency and MDC (Gas Proportional—α Only)

Surface Material	Density Thickness (mg/cm^2)	Th-230 (0.349 ± 0.015)[a]		
		Source Efficiency		MDC[d] (dpm/100 cm^2)
		Meas.[b]	Fit[c]	
Detector Face[e]	0.4	NA	NA	30
Detector Face[f] Plus 2 Sheets of Mylar	0.84	0.509	0.428 ± 0.215	34
Plus 2.28 mg/cm^2 Dust[g]	3.12	0.145	0.201 ± 0.071	120
Plus 4.11 mg/cm^2 Dust	4.95	0.134	0.110 ± 0.031	130
Plus 6.10 mg/cm^2 Dust	6.94	0.056	0.057 ± 0.016	310
Plus 7.99 mg/cm^2 Dust	8.83	0.026	0.030 ± 0.011	674
Plus 9.99 mg/cm^2 Dust	10.83	0.018	0.016 ± 0.008	974
Regression Equation		$\epsilon_s = 0.565\ e^{-0.331\ x}$		

[a]Instrument efficiency provided in parentheses; uncertainties represent the 95% confidence interval.
[b]Source efficiency was determined by dividing the total efficiency by the instrument efficiency.
[c]The measured source efficiency versus density thickness was fit to an exponential curve; uncertainties represent the 95% confidence interval.
[d]Probe area corrections of 126 cm^2 were made for the gas proportional detectors. The following MDC equation was used for 1-minute counts and a background of 1 cpm:

$$MDC = \frac{3 + 4.65\sqrt{C_B}}{KT}$$

[e]Measurements performed with a Ludlum 43-68 gas proportional detector with a standard 0.4-mg/cm^2 window.
[f]Each sheet of Mylar has a density thickness of 0.22 mg/cm^2.
[g]Dust obtained by grinding potting soil and sieving through 250 mesh screen.

Table 5.15 Effects of Dust Density Thickness on Source Efficiency and MDC (Gas Proportional—β Only)

Surface Material	Density Thickness (mg/cm^2)	C-14 (0.081 ± 0.002)[a]			Tc-99 (0.191 ± 0.016)			Tl-204 (0.355 ± 0.021)			SrY-90 (0.465 ± 0.024)		
		Source Efficiency		MDC[d] (dpm/100 cm^2)	Source Efficiency		MDC (dpm/100 cm^2)	Source Efficiency		MDC (dpm/100 cm^2)	Source Efficiency		MDC (dpm/100 cm^2)
		Meas[b]	Fit[c]		Meas.	Fit		Meas.	Fit		Meas.	Fit	
Detector Face[e]	3.8	NA	NA	1,823	NA	NA	577	NA	NA	280	NA	NA	222
Detector Face[f] Plus 2 Sheets of Mylar	4.24	0.435	0.448 ± 0.136	2,039	0.628	0.632 ± 0.061	599	0.715	0.715 ± 0.031	283	0.696	0.696 ± 0.028	222
Plus 2.28 mg/cm^2 Dust[g]	6.52	0.242	0.278 ± 0.060	3,659	0.501	0.519 ± 0.036	751	0.648	0.660 ± 0.020	312	0.649	0.665 ± 0.019	238
Plus 4.11 mg/cm^2 Dust	8.35	0.218	0.189 ± 0.033	4,074	0.479	0.443 ± 0.025	785	0.626	0.619 ± 0.015	323	0.655	0.641 ± 0.015	236
Plus 6.10 mg/cm^2 Dust	10.34	0.149	0.124 ± 0.022	5,957	0.371	0.373 ± 0.021	1,013	0.594	0.577 ± 0.014	340	0.627	0.617 ± 0.014	246
Plus 7.99 mg/cm^2 Dust	12.23	0.076	0.083 ± 0.018	11,680	0.305	0.317 ± 0.022	1,233	0.529	0.540 ± 0.017	382	0.593	0.594 ± 0.017	260
Plus 9.99 mg/cm^2 Dust	14.23	0.051	0.055 ± 0.016	17,243	0.270	0.267 ± 0.025	1,395	0.502	0.504 ± 0.021	403	0.564	0.571 ± 0.022	274
Regression Equation		$\epsilon_s = 1.10\ e^{-0.211\ x}$			$\epsilon_s = 0.912\ e^{-0.086\ x}$			$\epsilon_s = 0.830\ e^{-0.035\ x}$			$\epsilon_s = 0.757\ e^{-0.020\ x}$		

[a]Instrument efficiency provided in parentheses; uncertainties represent the 95% confidence interval.
[b]Source efficiency was determined by dividing the total efficiency by the instrument efficiency.
[c]The measured source efficiency versus density thickness was fit to an exponential curve; uncertainties represent the 95% confidence interval.
[d]Probe area corrections of 126 cm^2 were made for the gas proportional detectors. The following MDC equation was used for 1-minute counts and a background of 354 cpm:

$$MDC = \frac{3 + 4.65\sqrt{C_B}}{KT}$$

[e]Measurements performed with a Ludlum 43-68 gas proportional with a standard alpha-blocking 3.8-mg/cm^2 window.
[f]Each sheet of Mylar has a density thickness of 0.22 mg/cm^2.
[g]Dust obtained by grinding potting soil and sieving through 250 mesh screen.

Table 5.16 Effects of Dust Density Thickness on Source Efficiency and MDC (GM Detector)

Surface Material	Density Thickness (mg/cm^2)	C-14 (0.099 ± 0.002)[a]			Tc-99 (0.193 ± 0.021)			Tl-204 (0.278 ± 0.017)			SrY-90 (0.388 ± 0.020)		
		Measured Source Efficiency		MDC[d] (dpm/100 cm^2)	Source Efficiency		MDC (dpm/100 cm^2)	Source Efficiency		MDC (dpm/100 cm^2)	Source Efficiency		MDC (dpm/100 cm^2)
		Meas.[b]	Fit[c]		Meas.	Fit		Meas.	Fit		Meas.	Fit	
Detector Face[e]	---[f]	NA	NA	3,758	NA	NA	1,454	NA	NA	888	NA	NA	648
Detector Face[g] Plus 2 Sheets of Mylar	0.44	0.436	0.474 ± 0.176	4,098	0.627	0.642 ± 0.087	1,469	0.716	0.715 ± 0.015	894	0.697	0.706 ± 0.031	657
Plus 2.28 mg/cm^2 Dust[h]	2.72	0.257	0.291 ± 0.077	6,941	0.490	0.520 ± 0.050	1,877	0.658	0.661 ± 0.010	973	0.668	0.670 ± 0.021	686
Plus 4.11 mg/cm^2 Dust	4.55	0.234	0.196 ± 0.041	7,644	0.473	0.439 ± 0.034	1,949	0.617	0.621 ± 0.007	1,036	0.645	0.642 ± 0.016	710
Plus 6.10 mg/cm^2 Dust	6.54	0.160	0.128 ± 0.027	11,133	0.392	0.365 ± 0.028	2,345	0.590	0.580 ± 0.007	1,084	0.632	0.613 ± 0.015	725
Plus 7.99 mg/cm^2 Dust	8.43	0.080	0.085 ± 0.023	22,344	0.300	0.306 ± 0.030	3,067	0.543	0.543 ± 0.008	1,178	0.591	0.587 ± 0.019	776
Plus 9.99 mg/cm^2 Dust	10.43	0.049	0.056 ± 0.020	36,720	0.243	0.255 ± 0.034	3,789	0.504	0.507 ± 0.010	1,270	0.547	0.560 ± 0.024	838
Regression Equation		$\epsilon_s = 0.521\ e^{-0.215\ x}$			$\epsilon_a = 0.669\ e^{-0.093\ x}$			$\epsilon_s = 0.726\ e^{-0.034\ x}$			$\epsilon_s = 0.713\ e^{-0.023\ x}$		

[a]Instrument efficiency provided in parentheses; uncertainties represent the 95% confidence interval.

[b]Source efficiency was determined by dividing the total efficiency by the instrument efficiency.

[c]The measured source efficiency versus density thickness was fit to an exponential curve; uncertainties represent the 95% confidence interval.

[d]The following equation was used for 1 minute counts, with a background of 49 cpm and a probe area of 20 cm^2:

$$MDC = \frac{3 + 4.65\sqrt{C_B}}{KT}$$

[e]Measurements performed with an Eberline HP-260 GM detector with a standard mica window with typical thickness 1.4 to 2.0 mg/cm^2.

[f]Detector face is fixed part of detector and is not removable.

[g]Each sheet of Mylar has a density thickness of 0.22 mg/cm^2.

[h]Dust obtained by grinding potting soil and sieving through 250 mesh screen.

Table 5.17 Effects of Dust Density Thickness on Source Efficiency and MDC (ZnS Scintillation Detector)

Surface Material	Density Thickness (mg/cm^2)	Th-230 (0.259 ± 0.013)[a]		
		Source Efficiency		MDC[d] (dpm/100 cm^2)
		Meas.[b]	Fit[c]	
Detector Face[e]	---[f]	NA	NA	65
Detector Face[g] Plus 2 Sheets of Mylar	0.44	0.509	0.410 ± 0.327	78
Plus 2.28 mg/cm^2 Dust[h]	2.72	0.118	0.179 ± 0.092	340
Plus 4.11 mg/cm^2 Dust	4.55	0.109	0.092 ± 0.039	367
Plus 6.10 mg/cm^2 Dust	6.54	0.045	0.045 ± 0.024	885
Plus 7.99 mg/cm^2 Dust	8.43	0.023	0.022 ± 0.017	1,735
Plus 9.99 mg/cm^2 Dust	10.43	0.017[i]	NA	2,390
Regression Equation		$\epsilon_s = 0.481\ e^{-0.364\ x}$		

[a]Instrument efficiency provided in parentheses; uncertainties represent the 95% confidence interval.
[b]Source efficiency was determined by dividing the total efficiency by the instrument efficiency.
[c]The measured source efficiency versus density thickness was fit to an exponential curve; uncertainties represent the 95% confidence interval.
[d]The following MDC equation was used for 1-minute counts, with a background of 1 cpm and a probe area of 74 cm^2:

$$MDC = \frac{3 + 4.65\sqrt{C_B}}{KT}$$

[e]Measurements performed with an Eberline AC3-7 ZnS scintillation detector with a standard 1.5-mg/cm^2 window.
[f]Detector face is fixed part of detector and is not removable.
[g]Each sheet of Mylar has a density thickness of 0.22 mg/cm^2.
[h]Dust obtained by grinding potting soil and sieving through 250 mesh screen.
[i]Data point not used in regression fit due to limited alpha range.

Table 5.18 Effects of Water Density Thickness on Source Efficiency and MDC (Gas Proportional—α+β/C-14)

Surface Material	Density Thickness (mg/cm^2)	C-14 (0.139 ± 0.003)[a]		
		Source Efficiency		MDC[d] ($dpm/100\ cm^2$)
		Meas.[b]	Fit[c]	
Detector Face[e]	0.4	NA	NA	629
Detector Face Plus 2 Mylar Sheets With 1 Kimwipe[f]	2.70	0.436	0.442 ± 0.042	1,249
Plus 0.44 mg/cm^2 Water[g]	3.14	0.362	0.397 ± 0.035	1,502
Plus 0.62 mg/cm^2 Water	3.32	0.360	0.380 ± 0.032	1,513
Plus 0.78 mg/cm^2 Water	3.48	0.349	0.365 ± 0.030	1,558
Plus 1.23 mg/cm^2 Water	3.93	0.333	0.327 ± 0.025	1,637
Plus 2.29 mg/cm^2 Water	4.99	0.284	0.252 ± 0.017	1,920
Plus 3.04 mg/cm^2 Water	5.74	0.237	0.210 ± 0.014	2,297
Plus 5.14 mg/cm^2 Water	7.84	0.138	0.125 ± 0.011	3,940
Plus 6.49 mg/cm^2 Water	9.19	0.083	0.090 ± 0.010	6,533
Plus 7.62 mg/cm^2 Water	10.32	0.063	0.068 ± 0.009	8,599
Regression Equation		$\epsilon_s = 0.858\ e^{-0.245\ x}$		

[a]Instrument efficiency provided in parentheses; uncertainties represent the 95% confidence interval.
[b]Source efficiency was determined by dividing the total efficiency by the instrument efficiency.
[c]The measured source efficiency versus density thickness was fit to an exponential curve; uncertainties represent the 95% confidence interval.
[d]Probe area corrections of 126 cm^2 were made for the gas proportional detectors. The following MDC equation was used for 1-minute counts and a background of 396 cpm:

$$MDC = \frac{3 + 4.65\sqrt{C_B}}{KT}$$

[e]Measurements performed with a Ludlum 43-68 gas proportional detector with a standard 0.4 mg/cm^2 window.
[f]Each sheet of Mylar has a density thickness of 0.22 mg/cm^2 and one Kimwipe has a density thickness of 1.86 mg/cm^2.
[g]Reagent water used in analytical procedures from radiochemistry laboratory.

Table 5.19 Effects of Water Density Thickness on Source Efficiency and MDC (Gas Proportional— α+β/Tc-99)

Surface Material	Density Thickness (mg/cm^2)	Tc-99 (0.239 ± 0.020)[a]		
		Source Efficiency		MDC[d] ($dpm/100\ cm^2$)
		Meas.[b]	Fit[c]	
Detector Face[e]	0.4	NA	NA	368
Detector Face Plus 2 Mylar Sheets With 1 Kimwipe[f]	2.70	0.626	0.642 ± 0.020	506
Plus 0.19 mg/cm^2 Water[g]	2.89	0.628	0.630 ± 0.019	505
Plus 0.76 mg/cm^2 Water	3.46	0.595	0.596 ± 0.016	533
Plus 2.85 mg/cm^2 Water	5.55	0.501	0.487 ± 0.010	633
Plus 3.97 mg/cm^2 Water	6.67	0.443	0.436 ± 0.009	716
Plus 5.49 mg/cm^2 Water	8.19	0.386	0.377 ± 0.009	822
Plus 6.67 mg/cm^2 Water	9.37	0.327	0.336 ± 0.010	969
Plus 8.17 mg/cm^2 Water	10.87	0.287	0.290 ± 0.011	1,104
Regression Equation		$\epsilon_s = 0.834\ e^{-0.097\ x}$		

[a]Instrument efficiency provided in parentheses; uncertainties represent the 95% confidence interval.
[b]Source efficiency was determined by dividing the total efficiency by the instrument efficiency.
[c]The measured source efficiency versus density thickness was fit to an exponential curve; uncertainties represent the 95% confidence interval.
[d]Probe area corrections of 126 cm^2 were made for the gas proportional detectors. The following MDC equation was used for 1-minute counts and a background of 396 cpm:

$$MDC = \frac{3 + 4.65\sqrt{C_B}}{KT}$$

[e]Measurements performed with a Ludlum 43-68 gas proportional detector with a standard 0.4-mg/cm^2 window.
[f]Each sheet of Mylar has a density thickness of 0.22 mg/cm^2 and one Kimwipe has a density thickness of 1.86 mg/cm^2.
[g]Reagent water used in analytical procedures from radiochemistry laboratory.

Table 5.20 Effects of Water Density Thickness on Source Efficiency and MDC (Gas Proportional—α+β/SrY-90)

Surface Material	Density Thickness (mg/cm^2)	SrY-90 (0.484 ± 0.025)[a]		
		Source Efficiency		MDC[d] ($dpm/100\ cm^2$)
		Meas.[b]	Fit[c]	
Detector Face[e]	0.4	NA	NA	207
Detector Face Plus 2 Mylar Sheets With 1 Kimwipe[f]	2.70	0.697	0.705 ± 0.018	225
Plus 2.56 mg/cm^2 Water[g]	5.26	0.666	0.664 ± 0.010	235
Plus 3.25 mg/cm^2 Water	5.95	0.666	0.653 ± 0.009	235
Plus 4.81 mg/cm^2 Water	7.51	0.627	0.630 ± 0.009	250
Plus 6.28 mg/cm^2 Water	8.98	0.608	0.608 ± 0.011	258
Plus 7.88 mg/cm^2 Water	10.58	0.582	0.586 ± 0.014	269
Regression Equation		$\epsilon_s = 0.751\ e^{-0.023\ x}$		

[a]Instrument efficiency provided in parentheses; uncertainties represent the 95% confidence interval.
[b]Source efficiency was determined by dividing the total efficiency by the instrument efficiency.
[c]The measured source efficiency versus density thickness was fit to an exponential curve; uncertainties represent the 95% confidence interval.
[d]Probe area corrections of 126 cm^2 were made for the gas proportional detectors. The following MDC equation was used for 1-minute counts and a background of 396 cpm:

$$MDC = \frac{3 + 4.65\sqrt{C_B}}{KT}$$

[e]Measurements performed with a Ludlum 43-68 gas proportional detector with a standard 0.4-mg/cm^2 window.
[f]Each sheet of Mylar has a density thickness of 0.22 mg/cm^2 and one Kimwipe has a density thickness of 1.86 mg/cm^2.
[g]Reagent water used in analytical procedures from radiochemistry laboratory.

Table 5.21 Effects of Water Density Thickness on Source Efficiency and MDC (Gas Proportional—α-Only)

Surface Material	Density Thickness (mg/cm^2)	Th-230 (0.085 ± 0.005)[a]		
		Source Efficiency		MDC[d] (dpm/100 cm^2)
		Meas.[b]	Fit[c]	
Detector Face[e]	0.4	NA	NA	30
Detector Face Plus 2 Mylar Sheets With 1 Kimwipe[f]	2.70	0.508	0.516 ± 0.071	140
Plus 0.11 mg/cm^2 Water[g]	2.81	0.469	0.485 ± 0.065	151
Plus 0.25 mg/cm^2 Water	2.95	0.441	0.448 ± 0.058	161
Plus 0.48 mg/cm^2 Water	3.18	0.372	0.393 ± 0.048	191
Plus 1.23 mg/cm^2 Water	3.93	0.274	0.257 ± 0.027	259
Plus 2.03 mg/cm^2 Water	4.73	0.168	0.163 ± 0.016	423
Plus 3.51 mg/cm^2 Water	6.21	0.090	0.071 ± 0.009	787
Plus 4.23 mg/cm^2 Water	6.93	0.039	0.047 ± 0.007	1,827
Plus 5.88 mg/cm^2 Water	8.58	0.018	0.018 ± 0.004	3,983
Regression Equation		$\epsilon_s = 2.39\ e^{-0.567\ x}$		

[a]Instrument efficiency provided in parentheses; uncertainties represent the 95% confidence interval.
[b]Source efficiency was determined by dividing the total efficiency by the instrument efficiency.
[c]The measured source efficiency versus density thickness was fit to an exponential curve; uncertainties represent the 95% confidence interval.
[d]Probe area corrections of 126 cm^2 were made for the gas proportional detectors. The following MDC equation was used for 1-minute counts and a background of 1cpm:

$$MDC = \frac{3 + 4.65\sqrt{C_B}}{KT}$$

[e]Measurements performed with a Ludlum 43-68 gas proportional detector with a standard 0.4-mg/cm^2 window.
[f]Each sheet of Mylar has a density thickness of 0.22 mg/cm^2 and one Kimwipe has a density thickness of 1.86 mg/cm^2.
[g]Reagent water used in analytical procedures from radiochemistry laboratory.

Table 5.22 Effects of Water Density Thickness on Source Efficiency and MDC (Gas Proportional—β-Only/C-14)

Surface Material	Density Thickness (mg/cm^2)	C-14 (0.046 ± 0.001)[a]		
		Source Efficiency		MDC[d] ($dpm/100\ cm^2$)
		Meas.[b]	Fit[c]	
Detector Face[e]	3.8	NA	NA	1,869
Detector Face Plus 2 Mylar Sheets With 1 Kimwipe[f]	6.10	0.436	0.445 ± 0.041	3,544
Plus 0.44 mg/cm^2 Water[g]	6.54	0.367	0.399 ± 0.034	4,209
Plus 0.62 mg/cm^2 Water	6.72	0.358	0.382 ± 0.031	4,317
Plus 0.78 mg/cm^2 Water	6.88	0.354	0.367 ± 0.029	4,363
Plus 1.23 mg/cm^2 Water	7.33	0.338	0.329 ± 0.024	4,576
Plus 2.29 mg/cm^2 Water	8.39	0.282	0.253 ± 0.016	5,480
Plus 3.04 mg/cm^2 Water	9.14	0.239	0.210 ± 0.013	6,457
Plus 5.14 mg/cm^2 Water	11.24	0.136	0.125 ± 0.011	11,359
Plus 6.49 mg/cm^2 Water	12.59	0.084	0.090 ± 0.010	18,320
Plus 7.62 mg/cm^2 Water	13.72	0.063	0.068 ± 0.009	24,606
Regression Equation		$\epsilon_s = 2.01\ e^{-0.247\ x}$		

[a]Instrument efficiency provided in parentheses; uncertainties represent the 95% confidence interval.
[b]Source efficiency was determined by dividing the total efficiency by the instrument efficiency.
[c]The measured source efficiency versus density thickness was fit to an exponential curve; uncertainties represent the 95% confidence interval.
[d]Probe area corrections of 126 cm^2 were made for the gas proportional detectors. The following MDC equation was used for 1-minute counts and a background of 354 cpm:

$$MDC = \frac{3 + 4.65\sqrt{C_B}}{KT}$$

[e]Measurements performed with a Ludlum 43-68 gas proportional detector with a standard alpha-blocking 3.8-mg/cm^2 window.
[f]Each sheet of Mylar has a density thickness of 0.22 mg/cm^2 and one Kimwipe has a density thickness of 1.86 mg/cm^2.
[g]Reagent water used in analytical procedures from radiochemistry laboratory.

Table 5.23 Effects of Water Density Thickness on Source Efficiency and MDC (Gas Proportional—β-Only/Tc-99)

Surface Material	Density Thickness (mg/cm^2)	Tc-99 (0.148 ± 0.013)[a]		
		Source Efficiency		MDC[d] ($dpm/100\ cm^2$)
		Meas.[b]	Fit[c]	
Detector Face[e]	3.8	NA	NA	620
Detector Face Plus 2 Mylar Sheets With 1 Kimwipe[f]	6.10	0.626	0.643 ± 0.026	773
Plus 0.19 mg/cm^2 Water[g]	6.29	0.630	0.632 ± 0.025	769
Plus 0.74 mg/cm^2 Water	6.84	0.590	0.602 ± 0.022	821
Plus 2.85 mg/cm^2 Water	8.95	0.518	0.500 ± 0.013	934
Plus 3.97 mg/cm^2 Water	10.07	0.469	0.452 ± 0.012	1,033
Plus 5.49 mg/cm^2 Water	11.59	0.402	0.396 ± 0.012	1,206
Plus 6.67mg/cm^2 Water	12.77	0.357	0.356 ± 0.014	1,356
Plus 8.17 mg/cm^2 Water	14.27	0.300	0.312 ± 0.015	1,614
Regression Equation		$\epsilon_s = 1.10\ e^{-0.088\ x}$		

[a]Instrument efficiency provided in parentheses; uncertainties represent the 95% confidence interval.
[b]Source efficiency was determined by dividing the total efficiency by the instrument efficiency.
[c]The measured source efficiency versus density thickness was fit to an exponential curve; uncertainties represent the 95% confidence interval.
[d]Probe area corrections of 126 cm^2 were made for the gas proportional detectors. The following MDC equation was used for 1-minute counts and a background of 354 cpm:

$$MDC = \frac{3 + 4.65\sqrt{C_B}}{KT}$$

[e]Measurements performed with a Ludlum 43-68 gas proportional detector with a standard alpha-blocking 3.8-mg/cm^2 window.
[f]Each sheet of Mylar has a density thickness of 0.22 mg/cm^2 and one Kimwipe has a density thickness of 1.86 mg/cm^2.
[g]Reagent water used in analytical procedures from radiochemistry laboratory.

Table 5.24 Effects of Water Density Thickness on Source Efficiency and MDC (Gas Proportional—β-Only/SrY-90)

Surface Material	Density Thickness (mg/cm^2)	SrY-90 (0.429 ± 0.023)[a]		
		Source Efficiency		MDC[d] ($dpm/100\ cm^2$)
		Meas.[b]	Fit[c]	
Detector Face[e]	3.8	NA	NA	222
Detector Face Plus 2 Mylar Sheets With 1 Kimwipe[f]	6.10	0.697	0.700 ± 0.021	241
Plus 2.56 mg/cm^2 Water[g]	8.66	0.665	0.666 ± 0.013	252
Plus 3.25 mg/cm^2 Water	9.35	0.661	0.657 ± 0.011	253
Plus 4.81 mg/cm^2 Water	10.91	0.635	0.637 ± 0.011	264
Plus 6.28 mg/cm^2 Water	12.38	0.632	0.619 ± 0.013	265
Plus 7.88 mg/cm^2 Water	13.98	0.590	0.600 ± 0.017	284
Regression Equation		$\epsilon_s = 0.790\ e^{-0.020\ x}$		

[a]Instrument efficiency provided in parentheses; uncertainties represent the 95% confidence interval.
[b]Source efficiency was determined by dividing the total efficiency by the instrument efficiency.
[c]The measured source efficiency versus density thickness was fit to an exponential curve; uncertainties represent the 95% confidence interval.
[d]Probe area corrections of 126 cm^2 were made for the gas proportional detectors. The following MDC equation was used for 1-minute counts and a background of 354 cpm:

$$MDC = \frac{3 + 4.65\sqrt{C_B}}{KT}$$

[e]Measurements performed with a Ludlum 43-68 gas proportional detector with a standard alpha-blocking 3.8-mg/cm^2 window.
[f]Each sheet of Mylar has a density thickness of 0.22 mg/cm^2 and one Kimwipe has a density thickness of 1.86 mg/cm^2.
[g]Reagent water used in analytical procedures from radiochemistry laboratory.

Table 5.25 Effects of Water Density Thickness on Source Efficiency and MDC (GM Detector/C-14)

Surface Material	Density Thickness (mg/cm^2)	C-14 (0.056 ± 0.001)[a]		
		Source Efficiency		MDC[d] ($dpm/100\ cm^2$)
		Meas.[b]	Fit[c]	
Detector Face[e]	---[f]	NA	NA	3,758
Detector Face Plus 2 Mylar Sheets With 1 Kimwipe[g]	2.30	0.436	0.494 ± 0.053	7,294
Plus 0.44 mg/cm^2 Water[h]	2.74	0.422	0.445 ± 0.044	7,526
Plus 0.62 mg/cm^2 Water	2.92	0.412	0.427 ± 0.041	7,716
Plus 0.78 mg/cm^2 Water	3.08	0.405	0.411 ± 0.038	7,847
Plus 1.23 mg/cm^2 Water	3.53	0.382	0.369 ± 0.032	8,320
Plus 2.29 mg/cm^2 Water	4.59	0.320	0.287 ± 0.021	9,925
Plus 3.04 mg/cm^2 Water	5.34	0.277	0.241 ± 0.018	11,481
Plus 5.14 mg/cm^2 Water	7.44	0.162	0.146 ± 0.015	19,622
Plus 6.49 mg/cm^2 Water	8.79	0.104	0.106 ± 0.014	30,496
Plus 7.62 mg/cm^2 Water	9.92	0.071	0.082 ± 0.013	44,680
Regression Equation		$\epsilon_s = 0.851\ e^{-0.236\ x}$		

[a]Instrument efficiency provided in parentheses; uncertainties represent the 95% confidence interval.
[b]Source efficiency was determined by dividing the total efficiency by the instrument efficiency.
[c]The measured source efficiency versus density thickness was fit to an exponential curve; uncertainties represent the 95% confidence interval.
[d]The following MDC equation was used for 1-minute counts, with a background of 49 cpm and probe area of 20 cm^2:

$$MDC = \frac{3 + 4.65\sqrt{C_B}}{KT}$$

[e]Measurements performed with an Eberline HP-260 GM detector with a standard mica window, typical thickness 1.4 to 2.0 mg/cm^2.
[f]Detector face is fixed part of detector and is not removable.
[g]Each sheet of Mylar has a density thickness of 0.22 mg/cm^2 and one Kimwipe has a density thickness of 1.86 mg/cm^2.
[h]Reagent water used in analytical procedures from radiochemistry laboratory.

Table 5.26 Effects of Water Density Thickness on Source Efficiency and MDC (GM Detector/Tc-99)

Surface Material	Density Thickness (mg/cm^2)	Tc-99 (0.161 ± 0.018)[a]		
		Source Efficiency		MDC[d] ($dpm/100\ cm^2$)
		Meas.[b]	Fit[c]	
Detector Face[e]	---[f]	NA	NA	1,454
Detector Face Plus 2 Mylar Sheets With 1 Kimwipe[g]	2.30	0.627	0.631 ± 0.022	1,762
Plus 0.19 mg/cm^2 Water[h]	2.49	0.611	0.621 ± 0.021	1,805
Plus 0.76 mg/cm^2 Water	3.06	0.580	0.590 ± 0.018	1,902
Plus 2.85 mg/cm^2 Water	5.15	0.501	0.490 ± 0.011	2,204
Plus 3.97 mg/cm^2 Water	6.27	0.463	0.444 ± 0.010	2,383
Plus 5.49 mg/cm^2 Water	7.79	0.392	0.387 ± 0.010	2,814
Plus 6.67 mg/cm^2 Water	8.97	0.347	0.349 ± 0.012	3,179
Plus 8.17 mg/cm^2 Water	10.47	0.296	0.305 ± 0.013	3,731
Regression Equation		$\epsilon_s = 0.775\ e^{-0.089\ x}$		

[a]Instrument efficiency provided in parentheses; uncertainties represent the 95% confidence interval.
[b]Source efficiency was determined by dividing the total efficiency by the instrument efficiency.
[c]The measured source efficiency versus density thickness was fit to an exponential curve; uncertainties represent the 95% confidence interval.
[d]The following MDC equation was used for 1-minute counts, with a background of 49 cpm and probe area of 20 cm^2:

$$MDC = \frac{3 + 4.65\sqrt{C_B}}{KT}$$

[e]Measurements performed with an Eberline HP-260 GM detector with a standard mica window, typical thickness 1.4 to 2.0 mg/cm^2.
[f]Detector face is fixed part of detector and is not removable.
[g]Each sheet of Mylar has a density thickness of 0.22 mg/cm^2 and one Kimwipe has a density thickness of 1.86 mg/cm^2.
[h]Reagent water used in analytical procedures from radiochemistry laboratory.

Table 5.27 Effects of Water Density Thickness on Source Efficiency and MDC (GM Detector/SrY-90)

Surface Material	Density Thickness (mg/cm^2)	SrY-90 (0.373 ± 0.020)[a]		
		Source Efficiency		MDC[d] ($dpm/100\ cm^2$)
		Meas.[b]	Fit[c]	
Detector Face[e]	---[f]	NA	NA	648
Detector Face Plus 2 Mylar Sheets With 1 Kimwipe[g]	2.30	0.697	0.708 ± 0.029	684
Plus 2.56 mg/cm^2 Water[h]	4.86	0.678	0.676 ± 0.017	703
Plus 3.25 mg/cm^2 Water	5.55	0.678	0.668 ± 0.015	703
Plus 4.81 mg/cm^2 Water	7.11	0.665	0.649 ± 0.015	717
Plus 6.28 mg/cm^2 Water	8.58	0.620	0.632 ± 0.018	768
Plus 7.88 mg/cm^2 Water	10.18	0.608	0.613 ± 0.024	783
Regression Equation		$\epsilon_s = 0.739\ e^{-0.018\ x}$		

[a]Instrument efficiency provided in parentheses; uncertainties represent the 95% confidence interval.
[b]Source efficiency was determined by dividing the total efficiency by the instrument efficiency.
[c]The measured source efficiency versus density thickness was fit to an exponential curve; uncertainties represent the 95% confidence interval.
[d]The following MDC equation was used for 1-minute counts, with a background of 49 cpm and probe area of 20 cm^2:

$$MDC = \frac{3 + 4.65\sqrt{C_B}}{KT}$$

[e]Measurements performed with an Eberline HP-260 GM detector with a standard mica window, typical thickness 1.4 to 2.0 mg/cm^2.
[f]Detector face is fixed part of detector and is not removable.
[g]Each sheet of Mylar has a density thickness of 0.22 mg/cm^2 and one Kimwipe has a density thickness of 1.86 mg/cm^2.
[h]Reagent water used in analytical procedures from radiochemistry laboratory.

Table 5.28 Effects of Water Density Thickness on Source Efficiency and MDC (ZnS Scintillation Detector)

Surface Material	Density Thickness (mg/cm^2)	Th-230 (0.069 ± 0.005)[a]		
		Source Efficiency		MDC[d] (dpm/100 cm^2)
		Meas.[b]	Fit[c]	
Detector Face[e]	---[f]	NA	NA	65
Detector Face Plus 2 Mylar Sheets With 1 Kimwipe[g]	2.30	0.508	0.453 ± 0.060	294
Plus 0.11 mg/cm^2 Water[h]	2.41	0.433	0.423 ± 0.054	345
Plus 0.25 mg/cm^2 Water	2.55	0.366	0.389 ± 0.048	407
Plus 0.48 mg/cm^2 Water	2.78	0.296	0.338 ± 0.040	504
Plus 1.23 mg/cm^2 Water	3.53	0.232	0.214 ± 0.021	645
Plus 2.03 mg/cm^2 Water	4.33	0.145	0.131 ± 0.012	1,030
Plus 3.51 mg/cm^2 Water	5.81	0.046	0.053 ± 0.006	3,265
Plus 4.23 mg/cm^2 Water	6.53	0.031	0.034 ± 0.005	4,814
Plus 5.88 mg/cm^2 Water	8.18	0.014	0.012 ± 0.003	10,465
Regression Equation		$\epsilon_s = 1.84\ e^{-0.610\ x}$		

[a]Instrument efficiency provided in parentheses; uncertainties represent the 95% confidence interval.
[b]Source efficiency was determined by dividing the total efficiency by the instrument efficiency.
[c]The measured source efficiency versus density thickness was fit to an exponential curve; uncertainties represent the 95% confidence interval.
[d]The following MDC equation was used for 1-minute counts, with a background of 1 cpm and probe area of 74 cm^2:

$$MDC = \frac{3 + 4.65\sqrt{C_B}}{KT}$$

[e]Measurements performed with an Eberline AC3-7 ZnS scintillation detector with a standard 1.5-mg/cm^2 window.
[f]Detector face is fixed part of detector and is not removable.
[g]Each sheet of Mylar has a density thickness of 0.22 mg/cm^2 and one Kimwipe has a density thickness of 1.86 mg/cm^2.
[h]Reagent water used in analytical procedures from radiochemistry laboratory.

Table 5.29 Total Efficiencies for Detectors Used To Assess Uranium Surface Activity

Radioactive Material (Surface Type)	Total Efficiency (counts per disintegration)[a]				
	Gas Proportional			GM	ZnS
	α Only[b]	β Only[c]	α + β[b]		
Processed Uranium[d]					
Stainless Steel	0.13	0.24	0.45	0.28	0.08
Concrete	0.10	0.22	0.44	0.19	0.06
Wood	0.04	0.21	0.32	0.22	0.02
Drywall	0.10	0.23	0.43	0.27	0.06
Enriched Uranium (3%)					
Stainless Steel	0.10	0.09	0.23	0.12	0.06
Concrete	0.07	0.07	0.18	0.10	0.05
Wood	0.06	0.08	0.17	0.10	0.03
Drywall	0.07	0.07	0.18	0.10	0.04
Ru-106 (Rh-106)					
Stainless Steel	---	0.55	0.57	0.56	---
Concrete	---	0.50	0.51	0.47	---
Wood	---	0.46	0.46	0.45	---
Drywall	---	0.35	0.34	0.30	---
SrY-90					
Stainless Steel	---	0.38	0.43	0.27	---
Concrete	---	0.34	0.38	0.23	---

[a]The total efficiencies were calculated by dividing net detector counts by radioactivity dispensed on the particular surface. All measurements were at contact with surface. For uranium, the alpha radioactivity (U-238, U-235, and U-234) was used. Activity was distributed over a 20 cm^2 area.
[b]Using window density thickness of 0.4 mg/cm^2.
[c]Using window density thickness of 3.8 mg/cm^2.
[d]Processed uranium includes U-238 in equilibrium with U-234, and U-235 present at natural isotopic ratios; the only other radionuclides present include the immediate progeny of U-238 and U-235.
[e]Data not obtained.

Table 5.30 Normalized Total Efficiencies for Processed Uranium With Various Absorber Thicknesses

Processed Uranium[a] on Stainless Steel With Mylar Absorber Thicknesses	Normalized Total Efficiency[b]				
	Gas Proportional			GM	ZnS
	α Only[c]	β Only[d]	α + β[c]		
No Mylar (at contact)	1.0	1.0	1.0	1.0	1.0
0.22 mg/cm^2 Mylar	0.85	1.0	0.96	1.0	0.69
0.44 mg/cm^2 Mylar	0.72	1.0	0.93	0.99	0.58
0.88 mg/cm^2 Mylar	0.53	1.0	0.90	0.97	0.33
1.32 mg/cm^2 Mylar	0.32	1.0	0.84	0.94	0.17
2.20 mg/cm^2 Mylar	0.05	0.98	0.77	0.90	0.03
3.30 mg/cm^2 Mylar	0.02	0.97	0.76	0.80	0.01

[a]Processed uranium includes U-238 in equilibrium with U-234, and U-235 present at natural isotopic ratios; the only other radionuclides present include the immediate progeny of U-238 and U-235.
[b]The total efficiencies were calculated by dividing net detector counts by radioactivity dispensed on the particular surface. Total efficiencies were then normalized to the total efficiency obtained with no Mylar. The alpha radioactivity U-238, U-235, and U-234) was distributed over a 20-cm^2 area.
[c]Using window density thickness of 0.4 mg/cm^2.
[d]Using window density thickness of 3.8 mg/cm^2.

Table 5.31 Detector Efficiency for Low Enriched Uranium (3%) Using a 126-cm^2 Proportional Detector With a 0.4 mg cm^{-2} Window (Gas Proportional—α + β)

Radionuclide	Radiation/Average Energy (MeV)	Alpha Fraction	Radiation Yield	Detection Efficiency	Weighted Efficiency
^{238}U	Alpha/4.2	0.167	100%	0.15	2.51×10^{-2}
^{234}Th	Beta/0.0435	0.167	100%	0.11	1.84×10^{-2}
^{234m}Pa	Beta/0.819	0.167	100%	0.49	8.17×10^{-2}
^{234}U	Alpha/4.7	0.799	100%	0.15	1.20×10^{-1}
^{235}U	Alpha/4.4	0.033	100%	0.15	5.00×10^{-3}
^{231}Th	Beta/0.0764	0.033	100%	0.22	7.27×10^{-3}
Total Weighted Efficiency					**0.257**

Table 5.32 Detector Efficiency for Low Enriched Uranium (3%) Using a 126-cm^2 Proportional Detector with a 3.8 mg cm^{-2} Window (Gas Proportional—β only)

Radionuclide	Radiation/Average Energy (MeV)	Alpha Fraction	Radiation Yield	Detection Efficiency	Weighted Efficiency
^{238}U	Alpha/4.2	0.167	100%	0.01	1.67×10^{-3}
^{234}Th	Beta/0.0435	0.167	100%	0.038	6.36×10^{-3}
^{234m}Pa	Beta/0.819	0.167	100%	0.453	7.58×10^{-2}
^{234}U	Alpha/4.7	0.799	100%	0.01	7.99×10^{-3}
^{235}U	Alpha/4.4	0.033	100%	0.01	3.33×10^{-4}
^{231}Th	Beta/0.0764	0.033	100%	0.118	3.93×10^{-3}
Total Weighted Efficiency					**0.096**

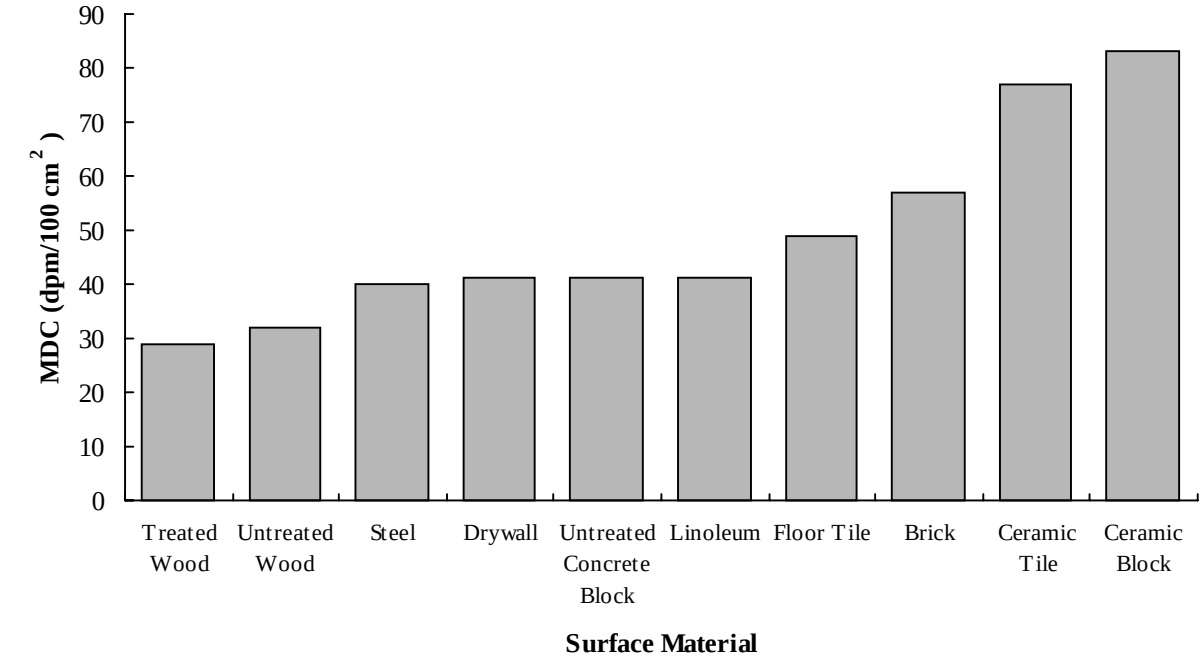

Figure 5.1: Effect of Surface Material on Gas Proportional Detector (α only) MDC

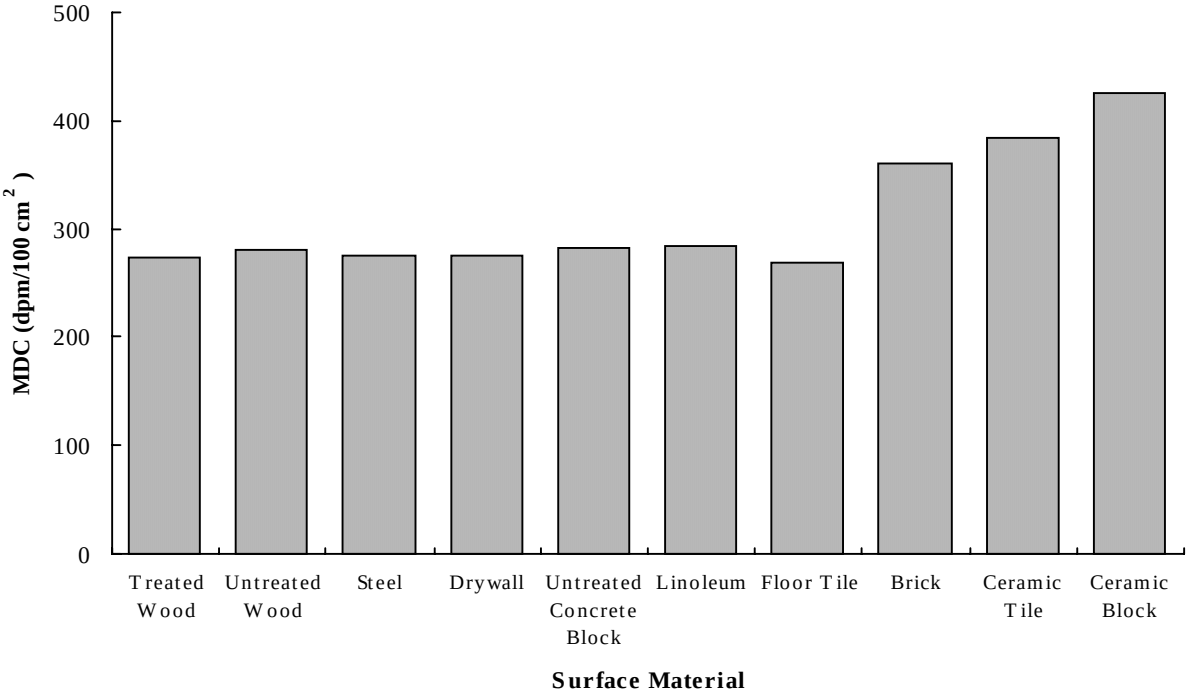

Figure 5.2: Effect of Surface Material on Gas Proportional Detector (β only) MDC

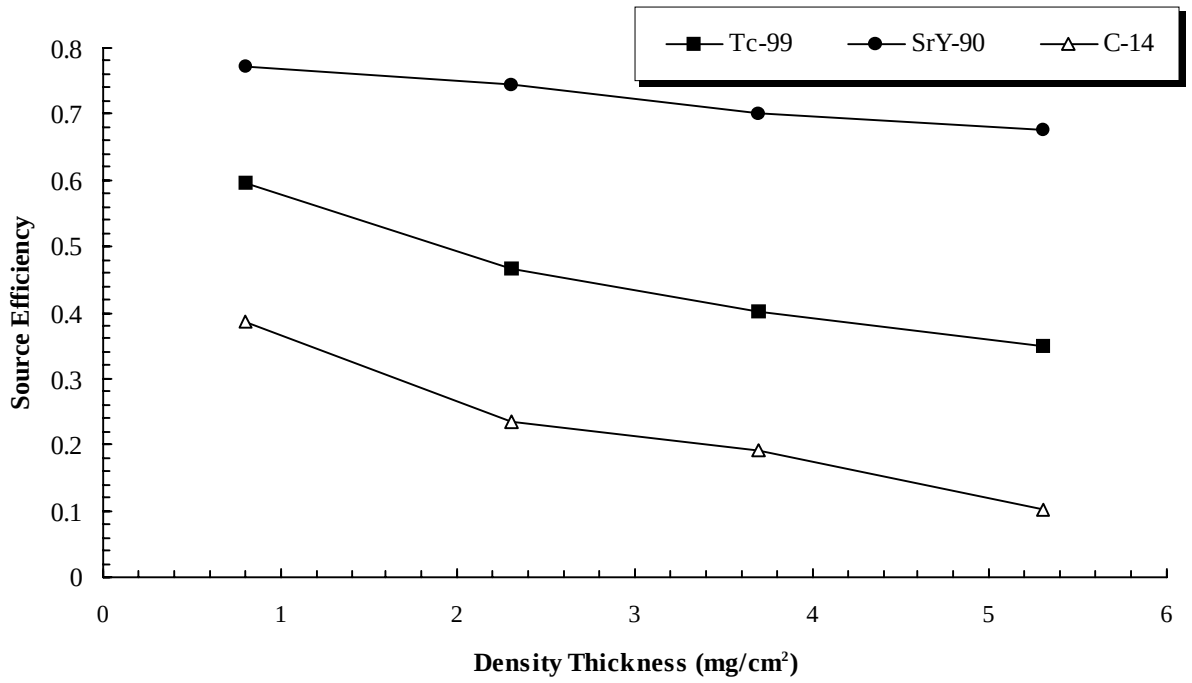

Figure 5.3: Effects of Oil Density Thickness on Source Efficiency for Various Sources

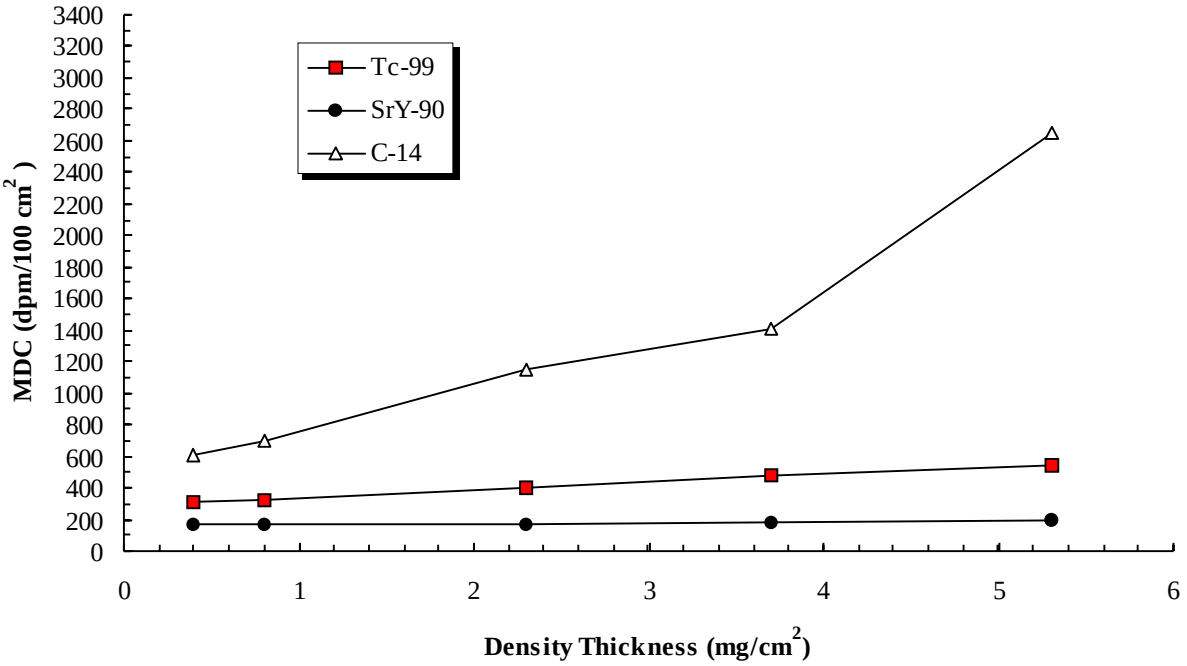

Figure 5.4: Effects of Oil Density Thickness on MDC

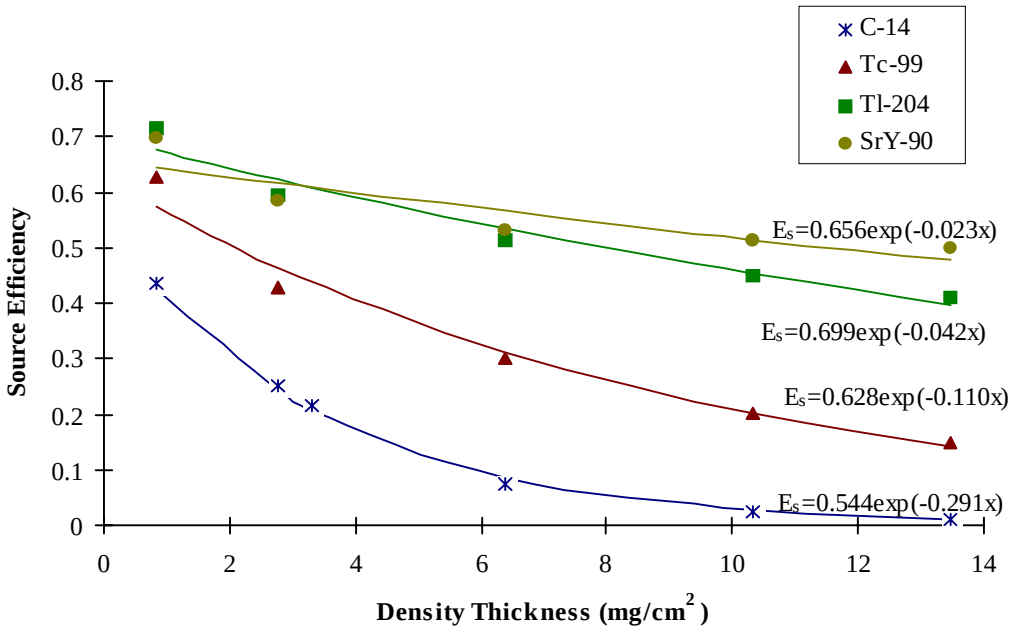

Figure 5.5: Effects of Paint Density Thickness on Source Efficiency (Gas Proportional—α+β)

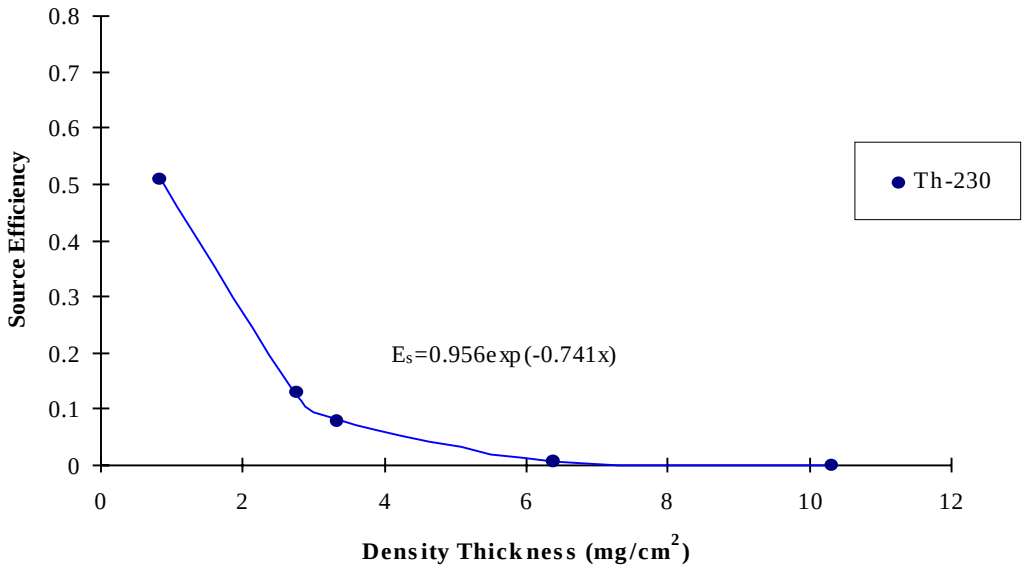

Figure 5.6: Effects of Paint Density Thickness on Source Efficiency (Gas Proportional—α only)

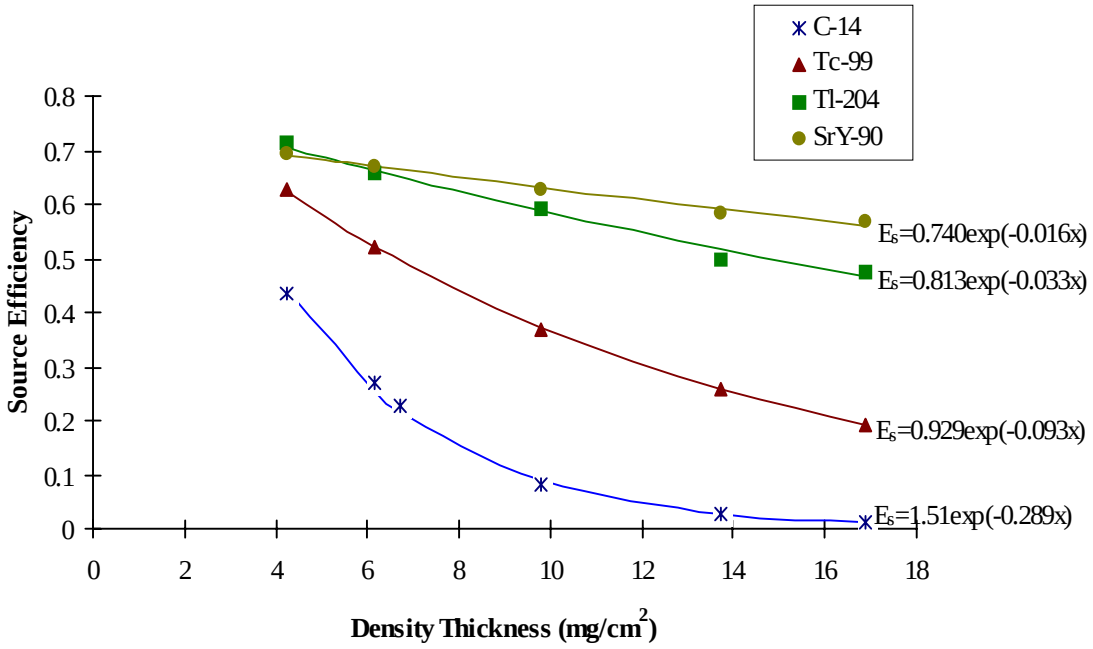

Figure 5.7: Effects of Paint Density Thickness on Source Efficiency (Gas Proportional—β only)

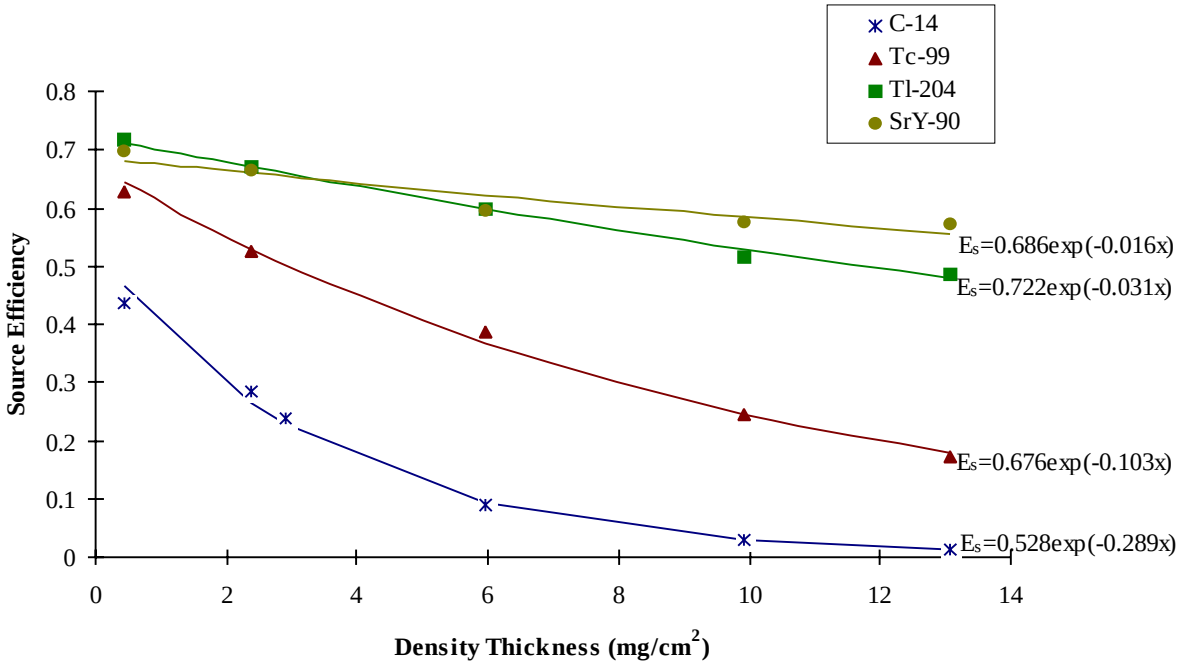

Figure 5.8: Effects of Paint Density Thickness on Source Efficiency (GM Detector)

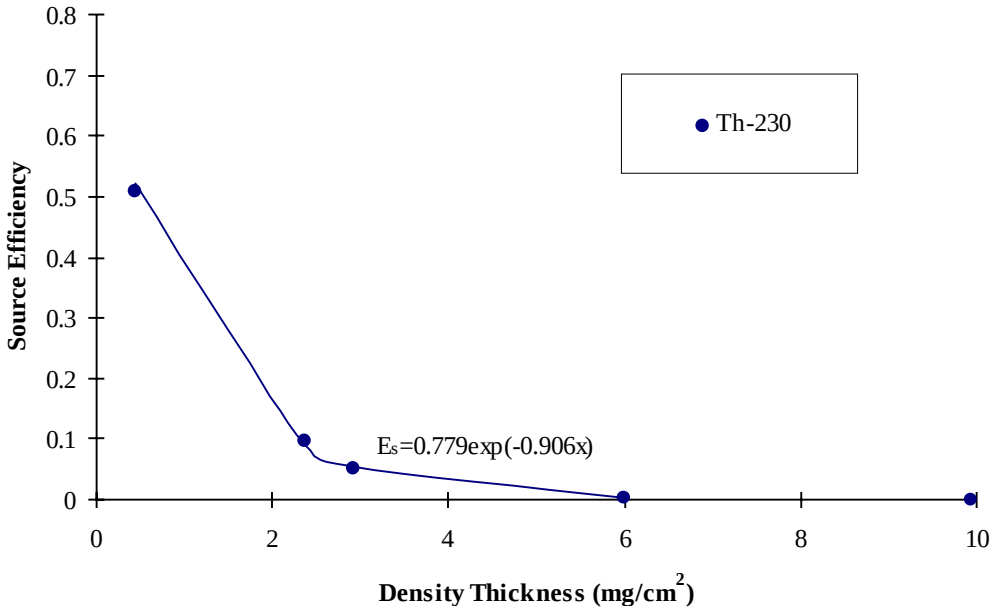

Figure 5.9: Effects of Paint Density Thickness on Source Efficiency (ZnS Scintillation Detector)

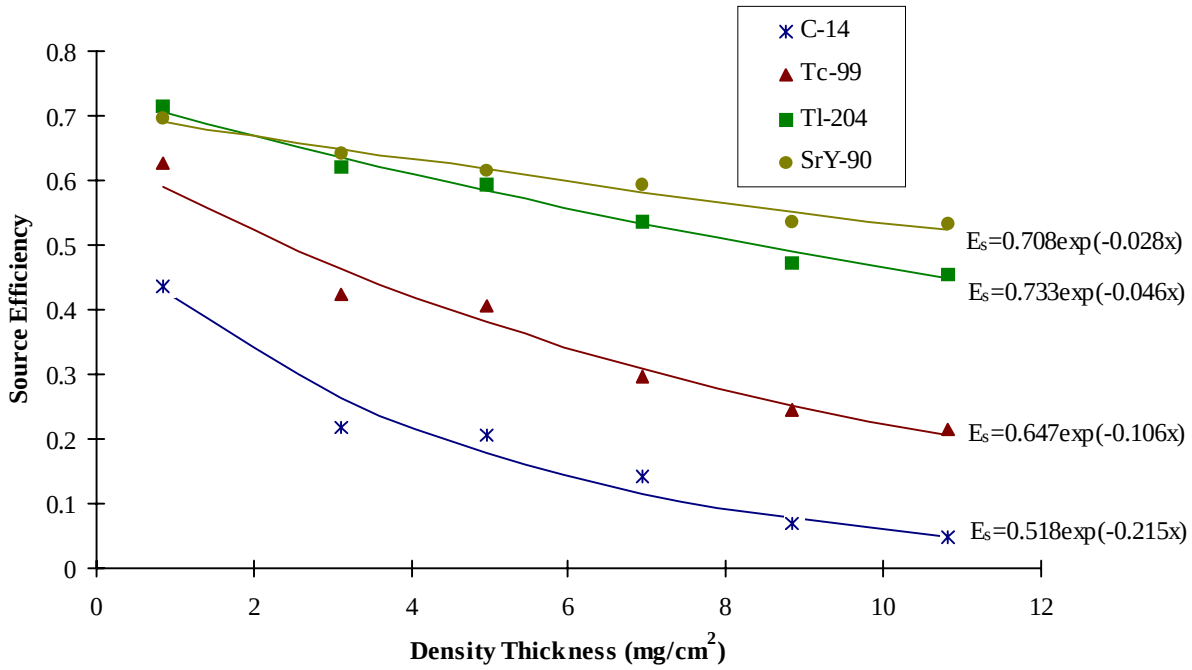

Figure 5.10: Effects of Dust Density Thickness on Source Efficiency (Gas Proportional—α+β)

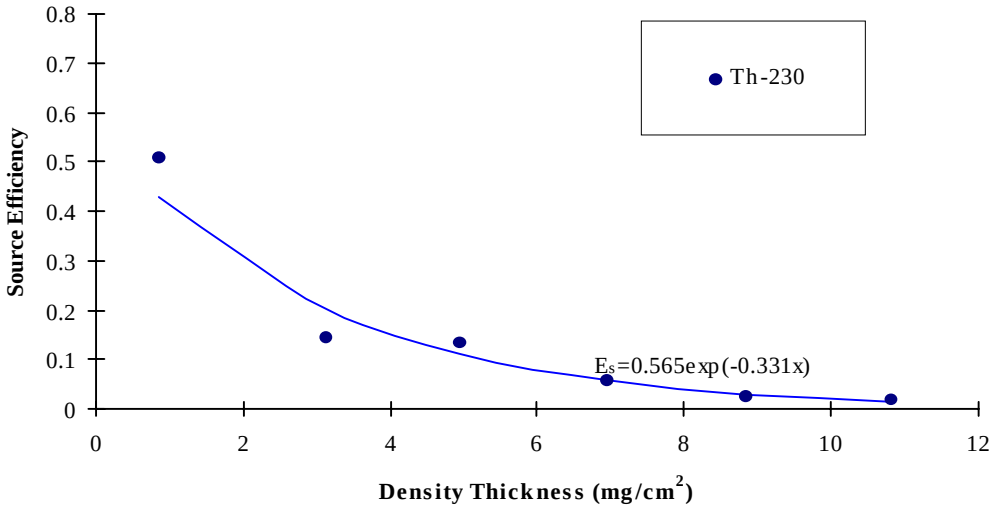

Figure 5.11: Effects of Dust Density Thickness on Source Efficiency (Gas Proportional—α only)

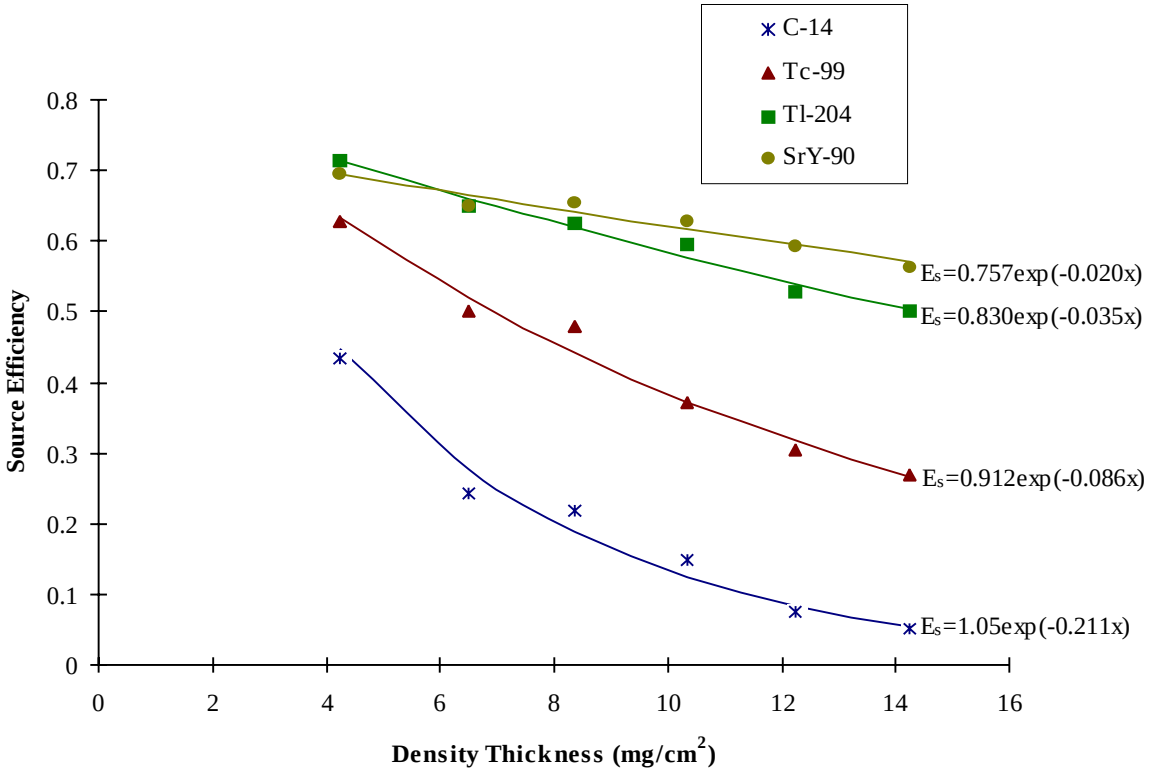

Figure 5.12: Effects of Dust Density Thickness on Source Efficiency (Gas Proportional—β only)

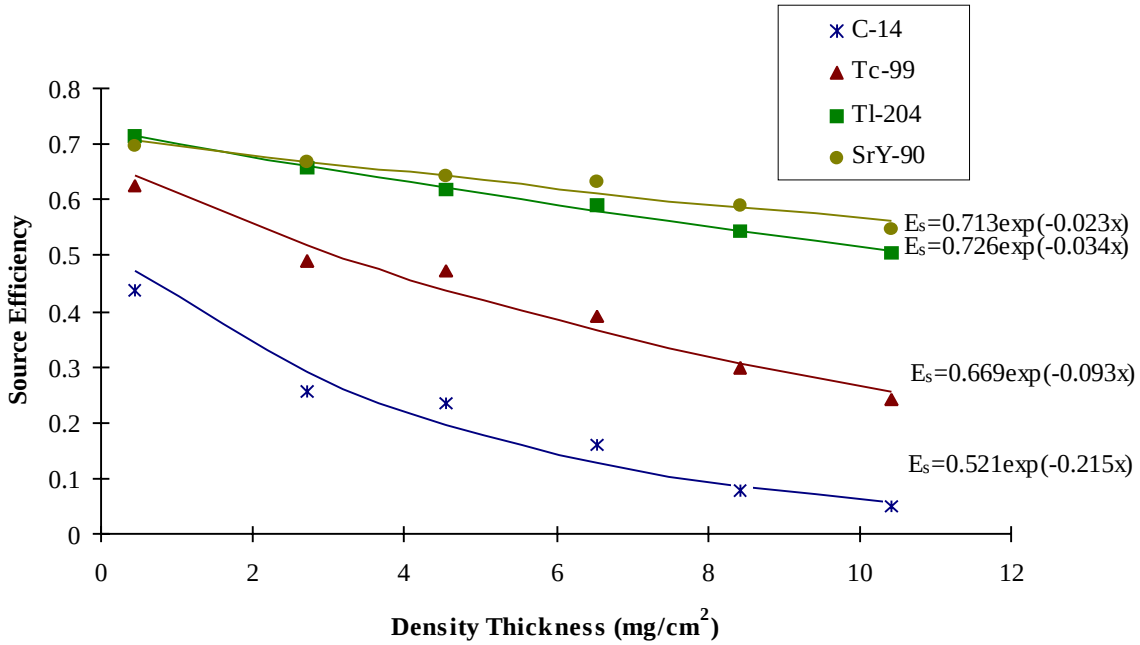

Figure 5.13: Effects of Dust Density Thickness on Source Efficiency (GM Detector)

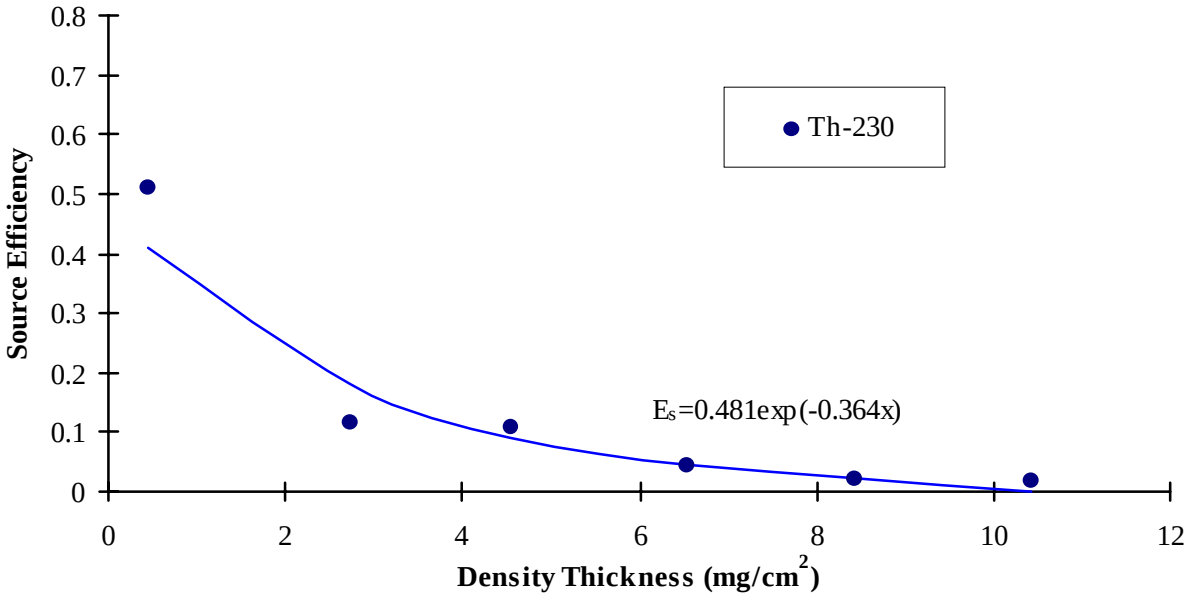

Figure 5.14: Effects of Dust Density Thickness on Source Efficiency (ZnS Scintillation Detector)

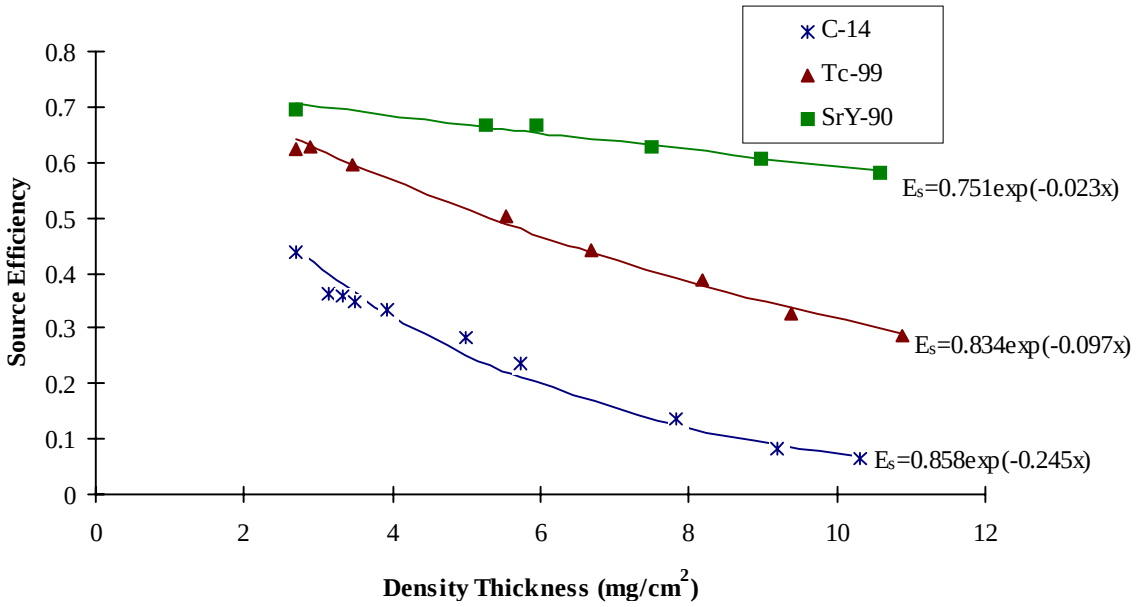

Figure 5.15: Effects of Water Density Thickness on Source Efficiency (Gas Proportional—α+β)

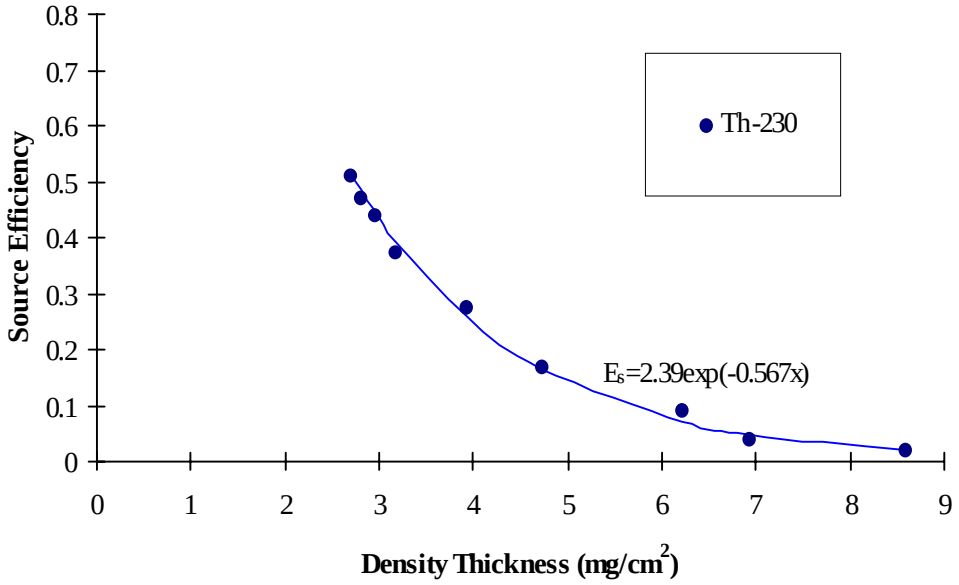

Figure 5.16: Effects of Water Density Thickness on Source Efficiency (Gas Proportional—α only)

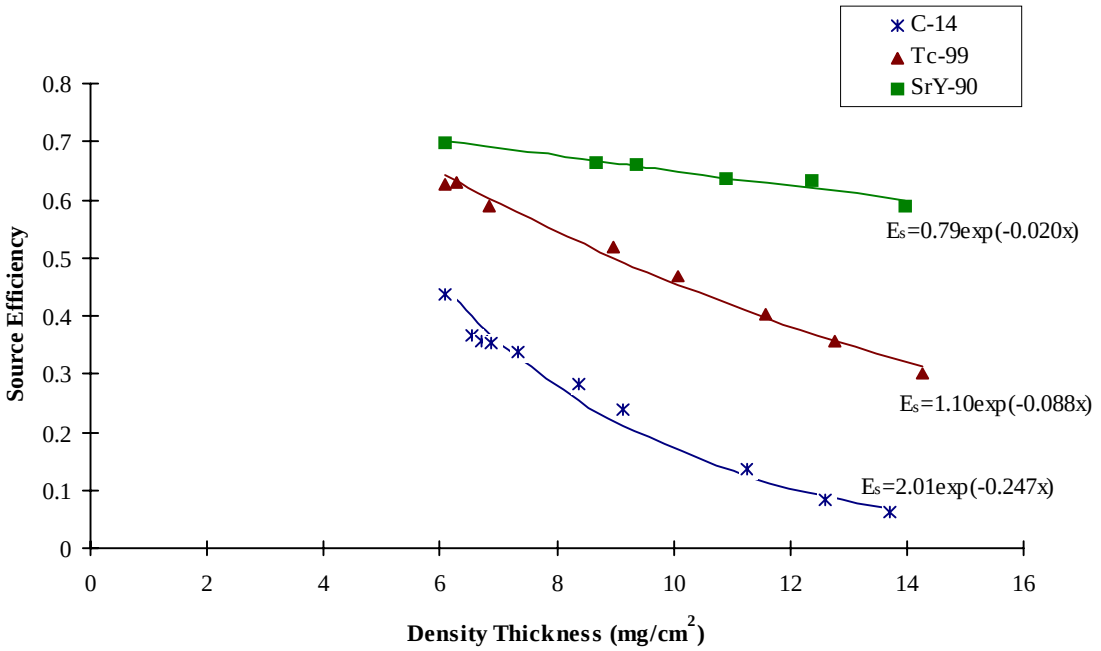

Figure 5.17: Effects of Water Density Thickness on Source Efficiency (Gas Proportional—β only)

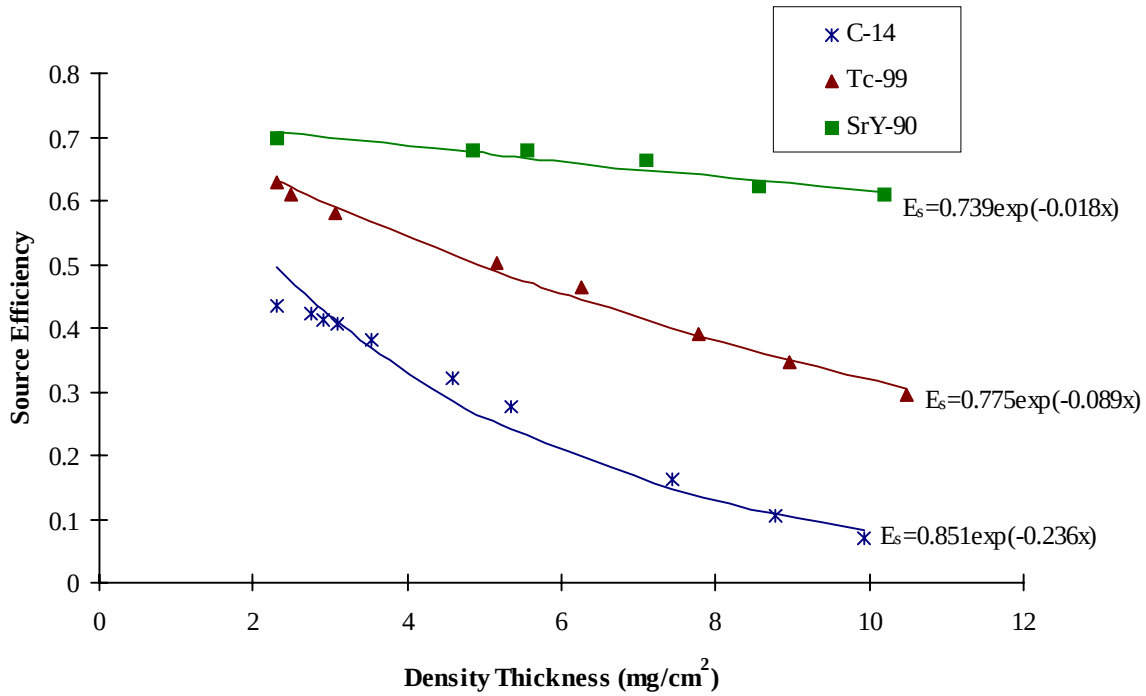

Figure 5.18: Effects of Water Density Thickness on Source Efficiency (GM Detector)

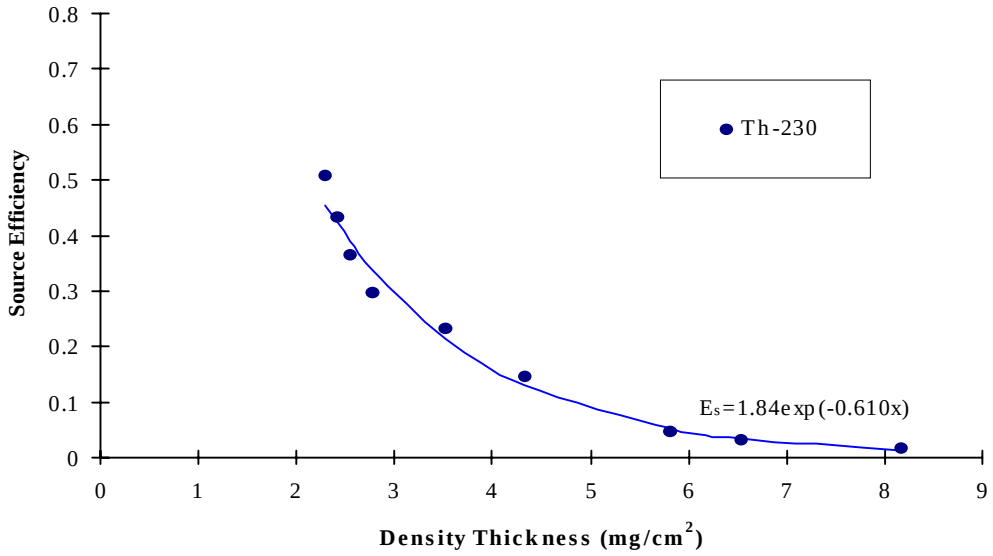

Figure 5.19: Effects of Water Density Thickness on Source Efficiency (ZnS Scintillation Detector)

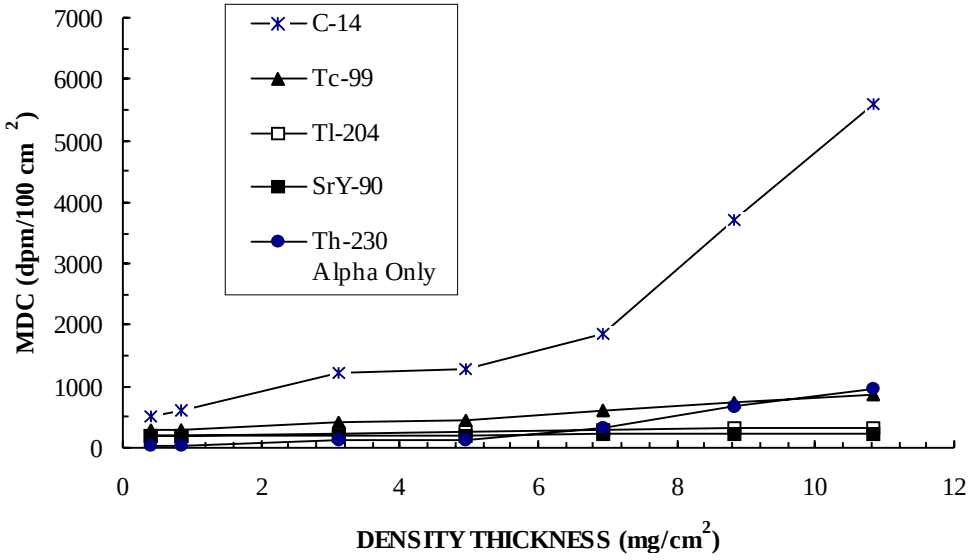

Figure 5.20: Effects of Dust Density Thickness on MDC for Various Sources Using the Gas Proportional Detector in α+β and α-Only Modes

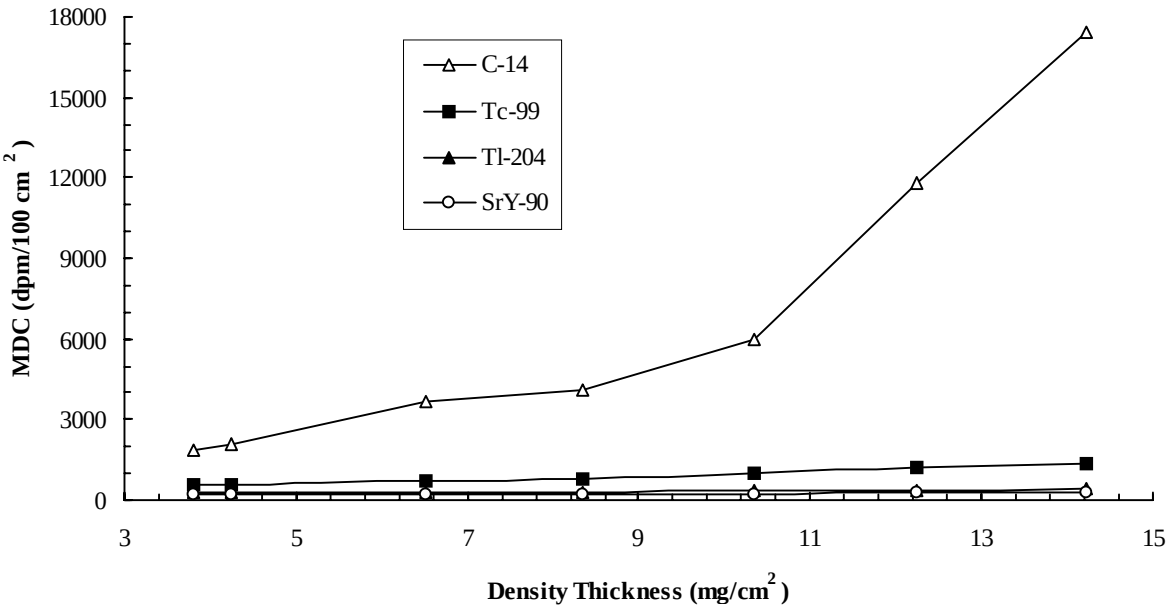

Figure 5.21: Effects of Dust Density Thickness on MDC for Various Sources Using the Gas Proportional in β-Only Mode

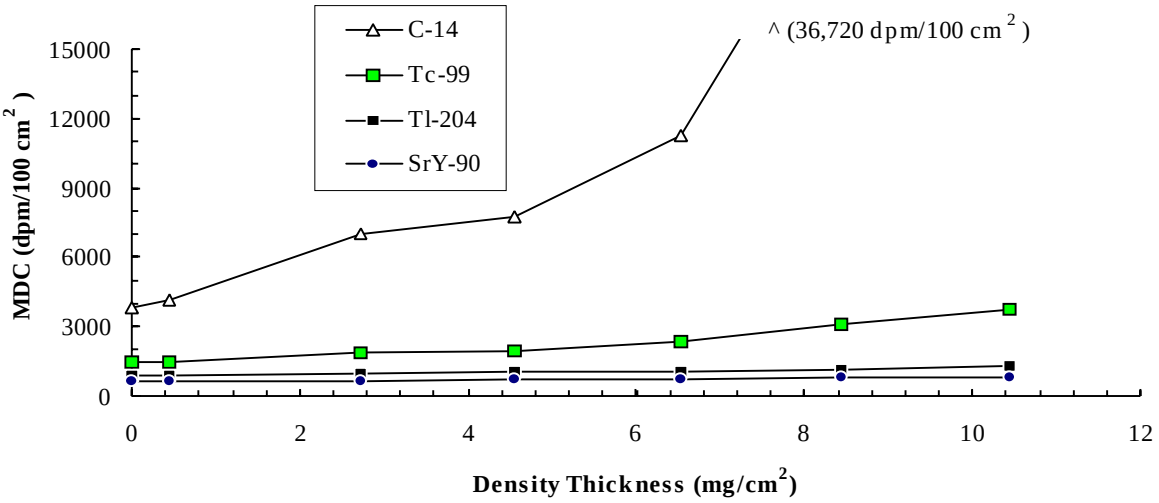

Figure 5.22: Effects of Dust Density Thickness on MDC for Various Sources Using the GM Detector

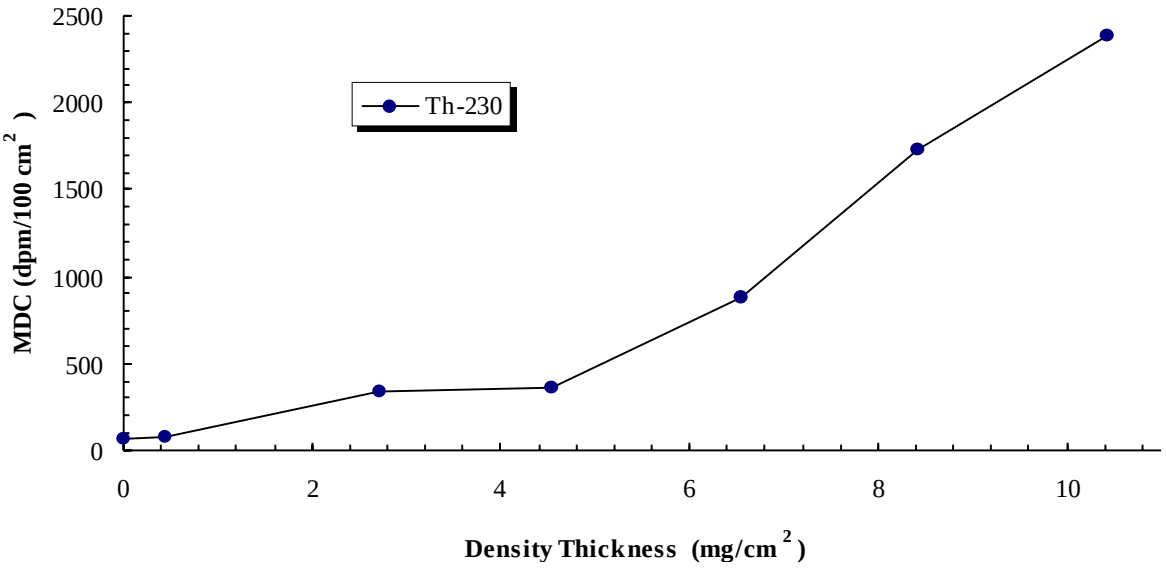

Figure 5.23: Effects of Dust Density Thickness on MDC for an Alpha Source Using the ZnS Scintillation Detector

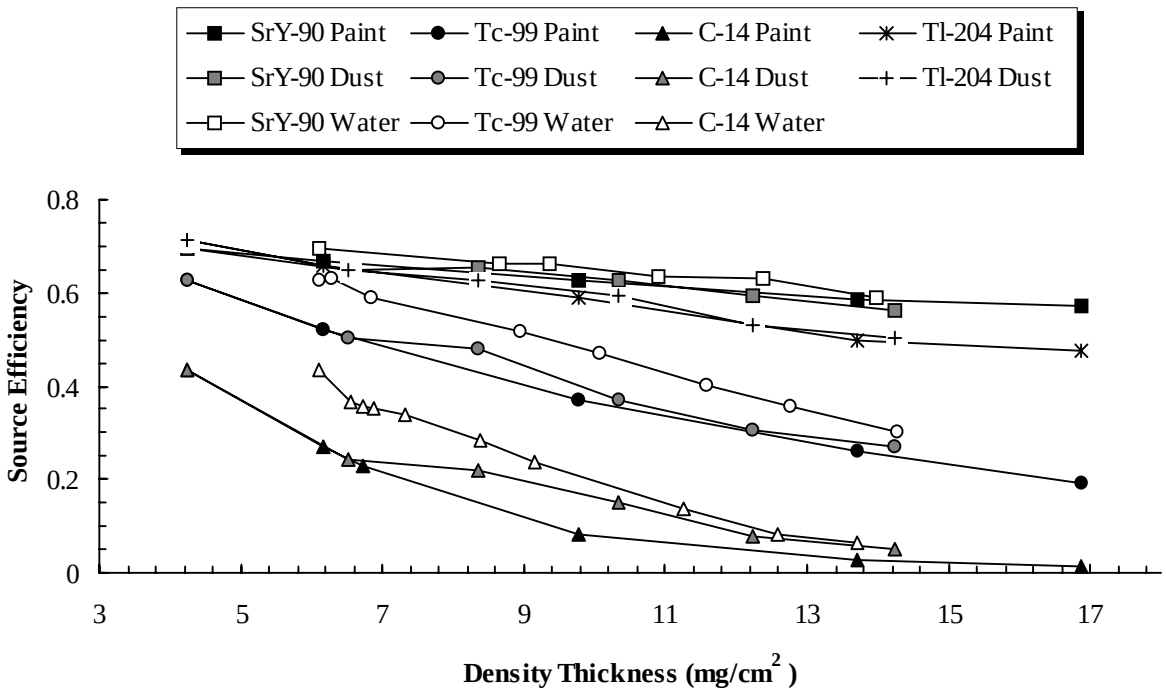

Figure 5.24: Overall Effects of Paint, Dust, and Water Density Thickness on Source Efficiency for Various Sources Using the Gas Proportional Detector in β–Only Mode